POLITECNICO DI TORINO

Dipartimento di Ingegneria Meccanica e Aerospaziale
Collegio di Ingegneria Meccanica, Aerospaziale, dell'Autoveicolo

Corso di laurea magistrale in
AUTOMOTIVE ENGINEERING (INGEGNERIA DELL'AUTOVEICOLO)

Master Thesis

Fracture toughness measurement using image correlation methods

Tutor

prof.
Paolo Matteis

Candidate

Matias Alejandro Valencia Zeballos

November 2024

Abstract

The J-integral is a fundamental parameter in fracture mechanics, representing the strain energy release rate around a crack tip. Traditional methods for measuring the J-integral rely on standardized mechanical testing procedures, involving complex loading and unloading procedures and post-processing of load-displacement data. This thesis explores the application of Digital Image Correlation (DIC) as a novel technique for calculating the J-integral. DIC is a non-contact optical method that provides full-field displacement and strain measurements with high spatial resolution. By capturing the deformation field around the crack tip, DIC allows for direct and real-time assessment of the J-integral.

The research presented in this thesis involves the development of a DIC-based methodology for J-integral calculation. The integration path was chosen so as to avoid large-strain regions and allow to determine the stress from the strain. The study also addresses discrepancies between the DIC approach and standard test methods, providing insights into the underlying reasons for these differences.

Results indicate that DIC offers a significant advantage in visualizing and analyzing crack tip fields, leading to a more comprehensive understanding of fracture behavior. However, challenges related to measurement sensitivity were identified, necessitating further refinement of the technique. Overall, this thesis demonstrates the potential of DIC as a powerful tool for J-integral calculation, potentially offering enhanced accuracy and efficiency for fracture toughness assessment in engineering materials.

Contents

Figures contents

Tables contents

1. Introduction

Fracture mechanics is a critical field of study in materials science and engineering, aiming to understand the behavior of materials under stress and predict the conditions under which they fail. One of the most important parameters in this field is the J-integral, which characterizes the strain energy release rate and provides a measure of the driving force on a crack tip in a material. Standard methods were developed using the integral that allowed the measurement of critical fracture properties in sample sizes that are too small for Linear Elastic Fracture Mechanics (LEFM) to be valid. These experiments allow the determination of fracture toughness from the critical value of fracture energy J_{Ic}, which defines the point at which ductile tearing and macroscopic crack propagation takes place under mode I loading.

Accurate determination of the J-integral is essential for predicting material failure and ensuring the safety and reliability of engineering structures.

Traditionally, the J-integral is measured using standardized mechanical testing methods, which involve applying a load to a pre-cracked specimen and recording the load-displacement response. These methods, while well-established, are often time-consuming and require complex instrumentation and/or complex loading and unloading procedures. Additionally, the accuracy of the J-integral calculation can be influenced by various factors, such as specimen geometry, loading conditions, and data interpretation techniques.

In recent years, advancements in optical measurement technologies have opened new avenues for improving the accuracy and efficiency of fracture mechanics testing. One such technology is Digital Image Correlation (DIC), a non-contact, optical method that measures full-field displacement and strain with high spatial resolution. DIC involves capturing a series of images of the specimen surface during loading and analyzing the changes in the speckle pattern to obtain displacement and strain fields on the specimen surface.

The application of DIC to the calculation of the J-integral presents some potential advantages over traditional methods. By providing detailed, real-time measurements of the deformation field around the crack tip, DIC potentially allows for a more comprehensive and direct assessment of the J-integral. However, the use of DIC also introduces new challenges, particularly regarding the calculation of the stress state in the plastic zone and the measure of the crack length.

This thesis aims to develop a method for calculating the J-integral using DIC and to evaluate its accuracy compared to standard test methods. For this purpose, a set of experimental data available from prior work [1], related to J_{IC} measurements on SENB (Single-Edge Notched Beam) specimens, is used. The J- Δa curve obtained using the standard test method is compared with the results obtained by the calculations from Digital Image Correlation.

The software, which is used to study the sequence of digital images, estimates the coordinates and displacements of all points on the surface of the test piece by solving a model-based optimization transport problem.

The DIC technique is based, in fact, on the comparison of two successive images of a component before and after being deformed. Deformations and displacements are thus calculated by considering and correlating the variation in position of blocks pixels between the reference image and the deformed image. The Image correlation process is based on the contrast between different shades of gray present on the sample.

A Digital Image Correlation Software (DICE [1]) was used to calculate the strain field on the specimen surface at different times. The calculated strain field was then used to calculate the J integral.

[1] DICe is an open-source digital image correlation (DIC) tool intended for use as a module in an external application or as a standalone analysis code. Its primary capabilities are computing full-field displacements and strains from sequences of digital images and rigid body motion tracking of objects. The images analyzed are typically of a material sample undergoing a characterization experiment, but DICe is also useful for other applications (for example, trajectory tracking).

2. Elastic-plastic fracture toughness testing

Linear elastic fracture mechanics is only valid as long as the plastic deformation is confined to a small region surrounding the tip of the crack. In many materials, however, it is not possible to effectively describe the fracture behavior with linear elastic fracture mechanics and one must use another model, elastic-plastic fracture mechanics. The two main Elastic-Plastic parameters that describe the conditions at the crack tip are the CTOD and the J integral. The main difference between J and CTOD as measures of toughness is that J is related to the area under the load-displacement curve whereas CTOD is related to the clip gage displacement. This means that the relationship between the two parameters depends on strain hardening and constraint [2].

2.1. CTOD measurement

There are various definitions of Crack Tip Opening Displacement. Among the most used there are the opening at the front of the crack and the displacement of the intersection of a 90-degree angle with the sides of the crack, as shown in Figure 1.

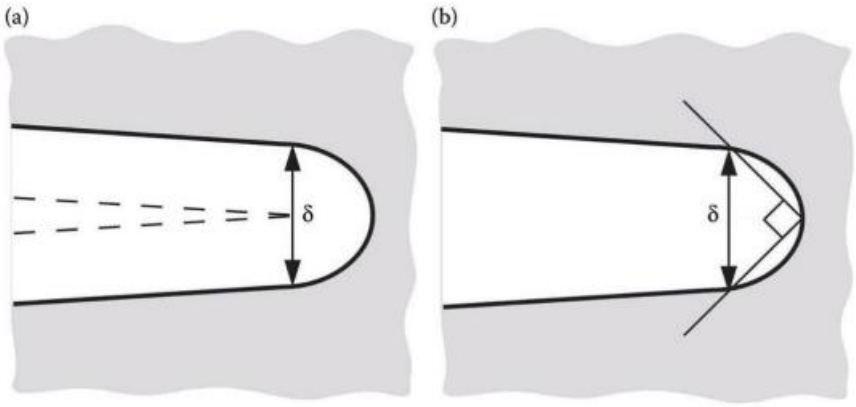

Figure 1. Alternative definitions of CTOD (a) Crack front opening (b) 90° intersection

It is possible to observe that the two definitions of CTOD (δ) are equivalent if the crack ends with semicircular (rounded) shape. In general, most of the tests in laboratory used to measure the CTOD are carried out with fracture toughness specimens loaded on three points (see Figure 2).

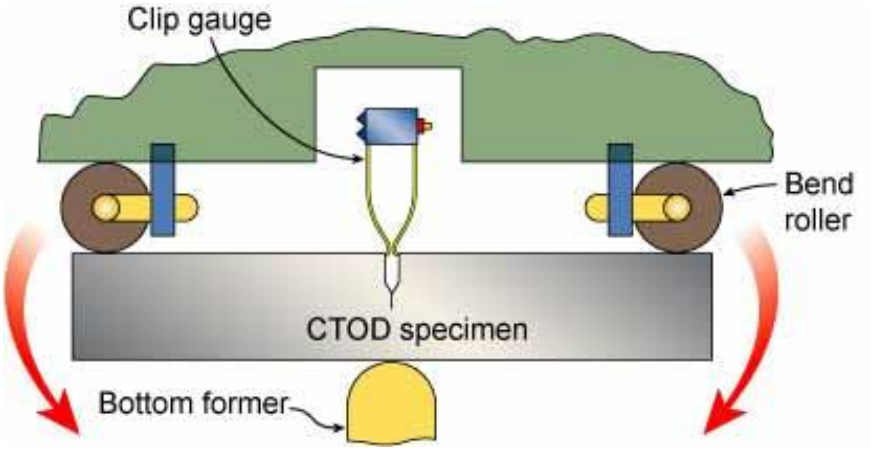

Figure 2. Typical test arrangement

Among the various techniques used to measure the CTOD, some have been developed based on digital image correlation.

In one method the first definition given of CTOD is considered (Figure 1(a)), which allows it to be measured from the relative displacements between the two faces of the crack. To obtain its value are considered the vertical displacements obtained experimentally. Figure 3 shows an example of the mapping of the vertical displacement.

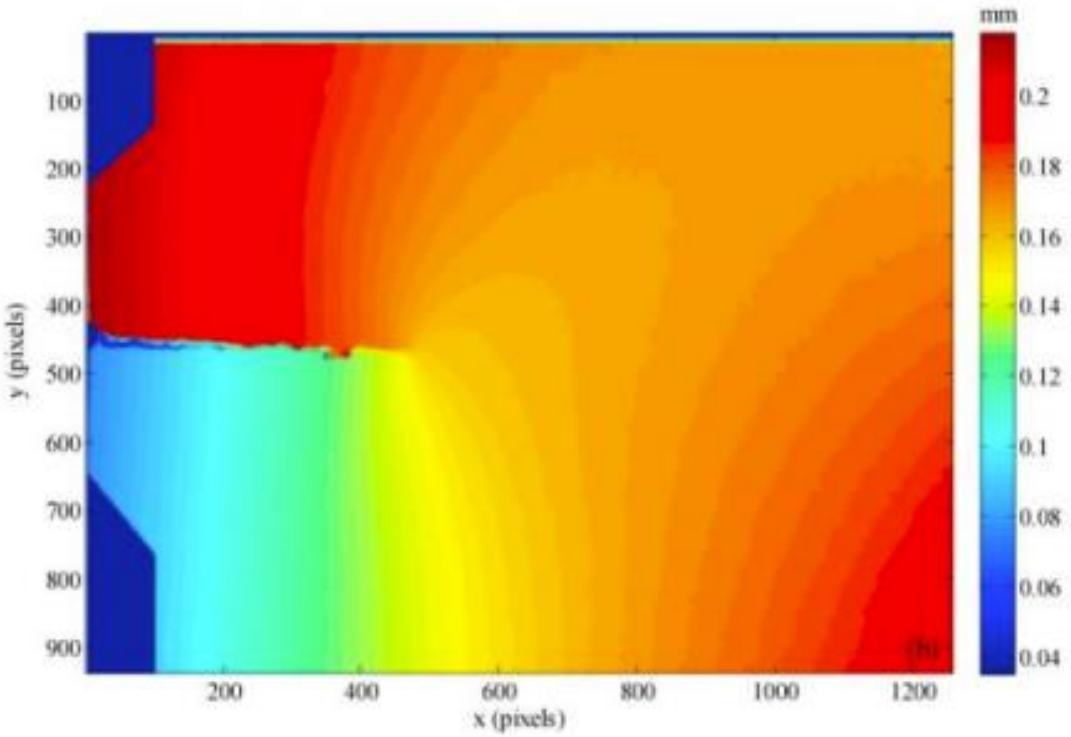

Figure 3. Vertical displacement measured with DIC [3]

After defining the graphic position of the crack tip, it is possible to calculate the CTOD. In order to obtain this, a pair of points are defined behind the apex of the crack and their movements relative to a loading and unloading cycle are analyzed [3]. The positions of the two points are indicated in terms of distance from the crack tip: Lx in crack propagation direction and Ly in the direction perpendicular to it, as can be seen in the enlargement in Figure 4.

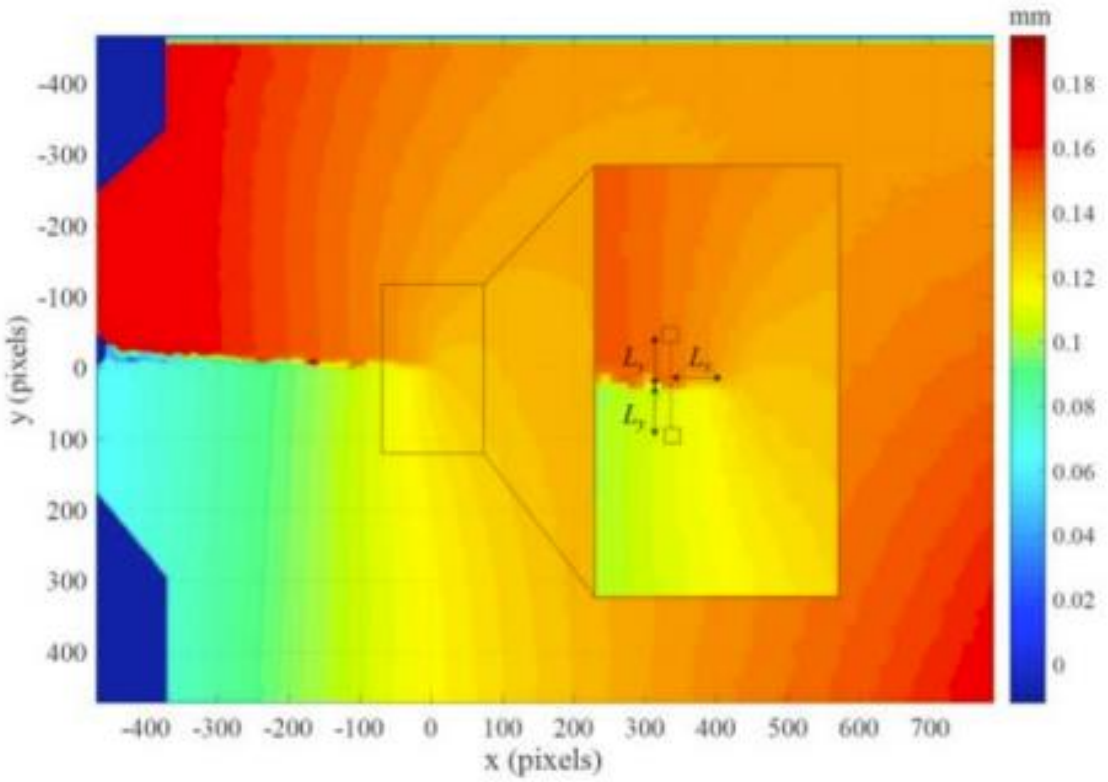

Figure 4. Enlargement on the pair of points chosen for the CTOD calculation [3]

2.2. The Integral J

The J-Integral equation was first introduced by Jim Rice in 1968 [4] and is probably the most fundamental quantity in nonlinear fracture mechanics. It is an integral equation that gives the amount of energy "released" per unit area of crack surface increase. It is the analog of Griffith's energy release rate [5], G, from LEFM (Linear Elastic Fracture Mechanics), though J is not limited to linear elastic analyses as G is.

Metals like steel exhibit elastic behavior for small loads. When the load is further increased the material can undergo plastic deformation. Such materials are called elastoplastic materials.

In a non-linear elastic model, the stress σ depends from the deformation ε in a biunivocal way. In a plastic-elastic model, instead, σ depends only from the elastic component of the deformation, while the plastic component of the deformation depends from the previous history and it is not in a biunivocal relation with σ.

The two models are approximately equivalent as long as the efforts increase monotonically, but they differ clearly when downloading as shown in Figure 5.

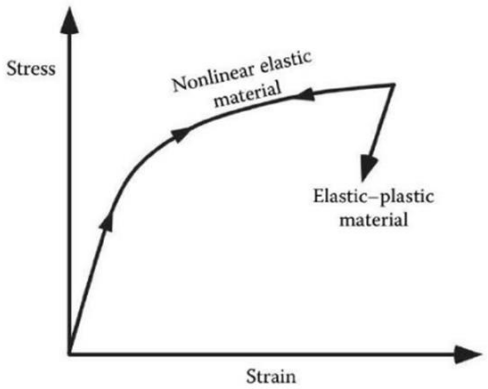

Figure 5. *Strain/Stress trend of non-linear elastic and elastic-plastic materials*

To characterize the fracture behavior of a non linear elastic plastic material, it is common to describe the fracture process with the help of the crack resistance curve (see Figure 6). The J-integral represents the energy released in a linear or nonlinear elastic material, due to an infinitesimal increase in crack length (Δa). Applying the J-Integral to materials which show elastic plastic deformation behavior requires some preconditions. Hence, several experimental methods exist to determine the crack resistance curve of mentioned non-linear elastic plastic materials.

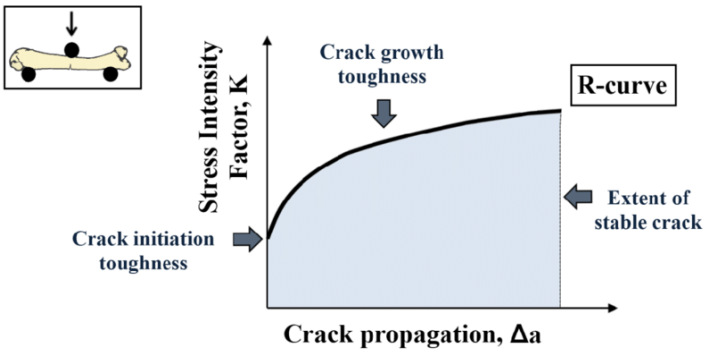

Figure 6. Crack resistance curve

J-integral theory is largely based on an elastic-nonlinear model; while metallic materials are correctly described only by an elastic-plastic model. Despite this, the elastic-nonlinear model is adopted because it allows a better approximation, compared to the simpler linear-elastic model.

2.2.1. First definition of J

To an increment of *dA* in the crack area generally follows an increment of the work of external forces dL_{est}, an increment of breaking work dL_{rot} and a variation in the elastic energy of the body dU_{el} (see Figure 7).

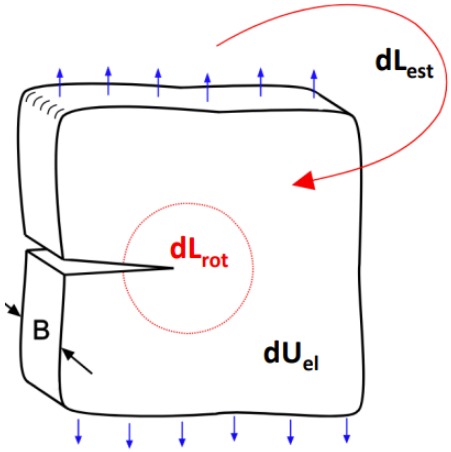

Figure 7. First definition of J

By applying the energy conservation:

$$dL_{est} = dL_{rot} + dU_{el} \qquad \text{Eq. 1}$$

The breaking work can be defined:

$$J = dL_{rot} / dA \qquad \text{Eq. 2}$$

Substituting the previous equality into Eq. 1 it is obtained:

$$J = - d/dA(U_{el} - L_{est}) \qquad \text{Eq. 3}$$

The quantity $U_{el} - L_{est}$ is defined as "potential energy", i.e. energy that is produced available when crack propagation occurs, so J is the amount of energy that is available for an infinitesimal advancement of the crack, in units of energy / area.

As a particular case, if the remote displacement is constant there is no work done by external forces ($dL_{ext}=0$) and so:

$$J = -\frac{dU}{dA} = -\frac{\partial}{\partial A}\int_0^v P dv \qquad \text{Eq. 4}$$

It immediately follows that, within the limits of linear elastic fracture mechanics, J = G (rate of release of elastic energy). Beyond the limits of linear elastic fracture mechanics however, in the real case (i.e. elastic-plastic and not elastic-non-linear), the deformation work can be recovered (or "released") only in part, because the plastic part is irrecoverable; therefore, G is no longer defined, while J takes on a different meaning.

2.2.2. Second definition of J

J is also defined with the following line integral in two dimensions, under the hypothesis of plane stress or plane strain, in a reference system where the crack is perpendicular to y and grows in direction x:

$$J = \int_{\Gamma} \left(w dy - T_i \frac{\partial u_i}{\partial x} ds \right) \qquad \text{Eq. 5}$$

where Γ is a path starting on one face of the crack and ending on the other, going around the apex, as shown in Figure 8; w is the elastic energy (or mechanical work of deformation) per unit volume, T is the local traction on a plane perpendicular to the unit vector n_j, and the same nj is perpendicular to Γ (locally) and always points outwards.

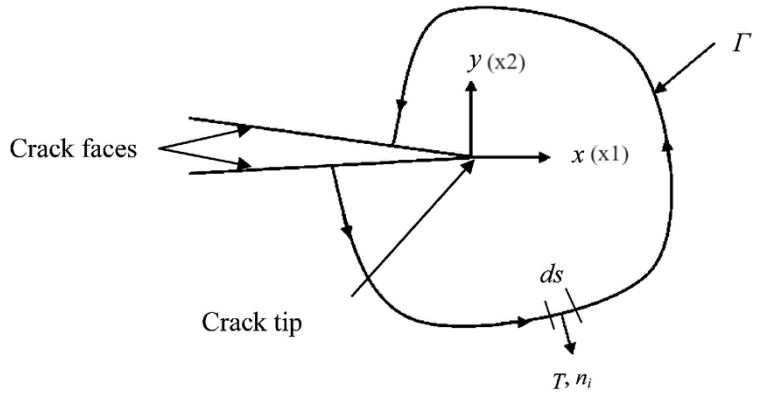

Figure 8. Flat surfaced notch in two-dimensional deformation field (all stresses depend only on x and y). Γ is any curve surrounding the notch tip.

The elastic energy w (in the linear elastic case) can be calculated as follows:

$$w = \int_0^{\varepsilon_{ij}} \sigma_{ij} * d\varepsilon_{ij} = \frac{1}{2}(\sigma_{xx}\varepsilon_{xx} + \sigma_{yy}\varepsilon_{yy} + 2\sigma_{xy}\varepsilon_{xy}) \qquad \text{Eq. 6}$$

And the traction T_i can be calculated as:

$$Ti = \sigma_{ij} * n_j \qquad \text{Eq. 7}$$

$$T_i = \sigma_{ij} * n_j = \sigma_{ix}n_x + \sigma_{iy}n_y = \begin{pmatrix} \sigma_{xx}n_x + \sigma_{xy}n_y \\ \sigma_{xy}n_x + \sigma_{yy}n_y \end{pmatrix} \qquad \text{Eq. 8}$$

2.2.3. Demonstrations

With the non-linear-elastic hypothesis, in the two-dimensional case (plane stress or plane strain), Rice demonstrated:

1. The integral J* calculated along a closed line Γ* (which does not contain singularities) is always zero.

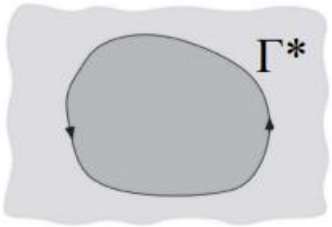

$$J^* = \int_{\Gamma^*} \left(w dy - T_i \frac{\partial u_i}{\partial x} ds \right) = 0$$

2. J calculated as a line integral is independent of the path chosen (as long as it starts on a face of the crack and ends on the other, going around the tip).

3. The two definitions of J (as a derivative of the deformation work and as a line integral) are always equivalent

Considering a homogeneus body of linear or nonlinear elastic material free of body forces and subjected to a two-dimensional deformation field (plane strain, generalized plane stress, antiplane strain) so that all stresses σ_{ij} depend only on two Cartesian coordinates x_1 (=x) and x_2 (=y). A straight crack is a limiting case for the demonstration, so it is considered a body containing a notch of the type shown in Figure 9, having flat surfaces parallel to the *x*-axis and a rounded tip [4].

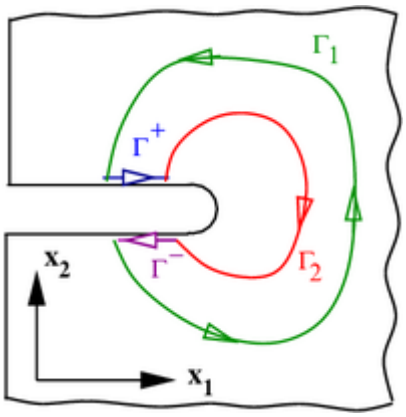

Figure 9. Line J-integral around a notch in two dimensions

The strain-energy density W is defined by

$$W = W(x,y) = W(e) = \int_0^{\varepsilon} \sigma_{ij} d\varepsilon_{ij} \qquad \text{Eq. 9}$$

Where $\varepsilon=[\varepsilon_{ij}]$ is the infinitesimal strain tensor. Considering now the integral J defined by Eq. 5 where Γ still represents a curve surrounding the notch tip, the integral being evaluated in a counterclockwise sense starting from the lower flat notch surface and continuing along the path Γ to the upper flat surface. T is the traction vector defined according to the out-ward normal along Γ, $T_i=\sigma_{ij}n_{ij}$, 'u' is the displacement vector and ds is an element of arc length along Γ. To prove path independent, it is considered any closed curve Γ^* enclosing an area A* in a two-dimensional deformation field free of body forces [4]. An application of Green's theorem gives

$$J = \int_{\Gamma*} \left(W dy - T \frac{\partial u_i}{\partial x} ds \right) = \int_{A*} [\frac{\partial W}{\partial x} - \frac{\partial}{\partial x_j} (\sigma_{ij} \frac{\partial u_i}{\partial x})] dx dy \qquad \text{Eq. 10}$$

Differentiating the strain energy density,

$$\frac{\partial W}{\partial x} = \frac{\partial W}{\partial e_{ij}} \frac{\delta \varepsilon_{ij}}{\delta x} = \sigma_{ij} \frac{\partial \varepsilon_{ij}}{\delta x} \qquad \text{Eq. 11}$$

$$= \frac{1}{2} \sigma_{ij} [\frac{\partial}{\partial x} \left(\frac{\partial u_i}{\partial x_j} \right) + \frac{\partial}{\partial x} (\frac{\partial u_j}{\partial x_i})]$$

$$= \sigma_{ij} \frac{\partial}{\partial x_j} \left(\frac{\partial u_i}{\partial x} \right) \quad (\text{since } \sigma_{ij} = \sigma_{ji})$$

$$= \frac{\partial}{\partial x_j} (\sigma_{ij} \frac{\partial u_i}{\partial x}) \quad (\text{since } \frac{\partial \sigma_{ij}}{\partial x_j} = 0)$$

The area integral in equation Eq. 10 vanishes identically, and thus

$$\int_{\Gamma*} \left(W dy - T \frac{\partial u_i}{\partial x} ds \right) = 0 \qquad \text{Eq. 12}$$

Considering any two paths Γ_1 and Γ_2 surrounding the notch tip as in Figure 9. Traversing Γ_1 in the counterclockwise sense, continuing along the upper flat notch surface to where Γ_2 intersects the notch, traversing Γ_2 in the clockwise sense, and then continuing along the lower flat notch surface to the starting point where Γ_1 intersects the notch. This describes a closed contour so that the integral of $\left(W dy - T \frac{\delta u}{\delta x} ds \right)$ vanishes. But T=0 and dy=0 on the portions of path along the flat notch surfaces. Thus, the integral along Γ_1 counterclockwise and the integral along Γ_2 clock-wise sum zero. J has the same value when computed by integrating along either Γ_1 or Γ_2 and path independence is proven (always assuming that the area between curves Γ_1 and Γ_2 is free of singularities) [4].

By taking Γ close to the notch tip can be made the integral depend only on the local field. The path could be shrunk to the tip of a smooth-ended notch and since T=0:

$$J = \int_{\Gamma} (W dy) \qquad \text{Eq. 13}$$

So that J is an averaged measure of the strain on the notch tip. The limit is not meaningful for a sharp crack. Nevertheless, since an arbitrarily small curve Γ may then be chosen surrounding the tip, the integral may be made to depend only on the crack tip singularity in the deformation field. The utility of the method rests in the fact that alternate choices of integration paths often permit a direct evaluation of J [4].

2.2.4. Principles of J_{IC}

The critical J-integral, denoted as J_{Ic}, is a fundamental parameter in fracture mechanics used to characterize the onset of crack growth in materials subjected to stress. It represents a measure of the strain energy release rate associated with crack initiation and is a critical indicator of a material's fracture toughness, especially under conditions where plastic deformation occurs before fracture (nonlinear elastic or elastic-plastic behavior). As such, J_{Ic} is particularly valuable in materials and structures expected to undergo significant plasticity near crack tips, providing a comprehensive approach for evaluating fracture resistance in ductile materials.

In essence, J_{Ic} quantifies the energy required per unit of crack extension in the presence of a stress field at the crack tip. It is defined as the critical value of the J-integral, J, at which stable crack initiation occurs under Mode I (opening mode) loading.

The J_{Ic} parameter is central to evaluating fracture toughness in engineering and materials science due to its ability to address conditions beyond the purely elastic assumptions of linear elastic fracture mechanics (LEFM). In materials prone to significant plasticity at the crack tip, LEFM parameters like K_{Ic} (stress intensity factor) may not adequately predict crack growth behavior. The J-integral, and particularly J_{Ic}, overcomes this limitation by accounting for elastic-plastic effects and providing a more realistic assessment of fracture initiation under complex stress states.

Experimental determination of JIc involves loading a precracked specimen (commonly single-edge bend [SE(B)], compact tension [C(T)], or disk-shaped compact [DC(T)] specimens) under controlled displacement. Loading is increased incrementally while simultaneously measuring load, displacement, and crack extension.

The multisample method, i.e. the use of several different samples to carry out the test, is expensive, because many must be pre-tested samples; therefore, it is rarely used (almost never). Instead, the single-sample method is used in practice and described here after.

During the test:

1. The basic procedure provides a single J_{Ic} value, utilizing optical crack size measurements at the initial loading stage.
2. The R-curve method yields a continuous resistance curve, J versus crack extension (Δa), to determine J_{Ic} as the point where stable crack growth initiates.

The exact value of J_{Ic} is identified as the intersection between a construction line (representing the initial crack resistance) and a 0.2 mm offset line from the J-Δa curve. This geometric method compensates for variations in plasticity, establishing J_{Ic} as a critical material constant indicating the onset of significant crack growth. To verify accuracy, a compliance calibration is often used, and multiple measurements ensure repeatability and reliability.

In practice, it serves as a robust indicator of material performance, particularly in applications where toughness and ductility are prioritized. It is used to:

- Rank materials for fracture resistance,
- Support material selection and quality control,
- Predict crack growth under loading conditions that include plastic deformation, and
- Guide flaw tolerance assessments in safety-critical structures.

Because J_{Ic} provides an intrinsic measure of a material's resistance to crack initiation under elastic-plastic deformation, it is instrumental in safety and reliability assessments, particularly for metals, polymers, and composites exposed to high-stress environments. The J_{Ic} metric also allows engineers to account for differences in laboratory and field conditions, making it highly applicable in structural integrity and life-prediction studies.

In summary, J_{Ic} is a critical fracture parameter in elastic-plastic fracture mechanics, essential for understanding and predicting the initiation of crack growth in ductile materials. Its definition, based on the J-integral, extends beyond the limitations of linear fracture mechanics, addressing the complexities of plastic deformation and making it invaluable in modern material and structural design.

3. Standard Test method for Measurement of J_{IC}

In this chapter it is introduced the methodology and procedures used to determine the fracture toughness of metallic materials, a critical parameter for assessing a material's resistance to crack propagation under stress. This assessment focuses on two key fracture behaviors: *fracture instability*, characterized by sudden, unstable crack extension, and *stable tearing*, where crack extension occurs progressively. These responses are identified through carefully controlled mechanical tests that yield critical toughness parameters, including K, J, and CTOD (crack-tip opening displacement), which characterize the material's resistance to different fracture scenarios.

The test methodology includes two main approaches: a *basic procedure* to measure a single fracture toughness value, and a *resistance curve (R-curve) procedure* for developing a continuous toughness versus crack extension relationship. Through these procedures, fracture properties can be evaluated under realistic loading conditions, providing valuable insights for material selection, quality control, and comparative studies within materials of similar yield strength.

The experimental setup consists of specialized fracture toughness testing equipment and single-edge bend (SE[B]), compact (C[T]), or disk-shaped compact (DC[T]) specimens. Each specimen contains a precracked notch to simulate realistic crack initiation and progression under controlled load conditions. By systematically applying incremental loading and partial unloading, compliance measurements allow for precise estimation of crack growth and crack-tip opening displacements, facilitating the construction of the R-curve.

Detailed calculations based on these measurements, such as compliance and J-integral values, are carried out to generate a fracture toughness curve, identifying the transition between stable tearing and the onset of plastic tearing. This rigorous approach allows for a comprehensive understanding of the material's crack growth resistance, which is essential for predicting performance in real-world applications.

The objective of this test method is to load a fatigue precracked test specimen to induce either or both of the following responses:

1. Unstable crack extension, including significant pop-in, referred to as "fracture instability."

2. Stable crack extension, referred to as "stable tearing".

Fracture instability results in a single point-value of fracture toughness determined at the point of instability. Stable tearing results in a continuous fracture toughness versus crack-extension relationship (R-curve) from which significant point-values may be determined (see Figure 6 as a reference of R-curve). Stable tearing interrupted by fracture instability results in an R-curve up to the point of instability [6].

Assuming the previously mentioned presence of a preexisting, sharp, fatigue crack, the material fracture toughness values identified by this test method characterize its resistance to:

1. Fracture of a stationary crack,
2. Fracture after some stable tearing,
3. Stable tearing onset, and
4. Sustained stable tearing.

This test method requires continuous measurement of force versus load-line displacement or crack mouth opening displacement, or both. If any stable tearing response occurs, then an R-curve is developed and the amount of slow-stable crack extension shall be measured [6].

Two alternative procedures for measuring crack extension are presented, the basic procedure and the resistance curve procedure. The basic procedure involves physical marking of the crack advance and multiple specimens used to develop a plot from which a single point initiation toughness value can be evaluated. The resistance curve procedure is an elastic-compliance method where multiple points are determined from a single specimen. In the latter case, high precision of signal resolution is required. These data can also be used to develop an R-curve [6].

3.1. Standard J_{IC} Test Method

The fracture toughness determined in accordance with this test method is for the opening mode (Mode I) of loading [6].

The recommended specimens can be single-edge bend, [SE(B)] (Figure 10(a)), compact, [C(T)] (Figure 10(b)), and disk-shaped compact, [DC(T)] (Figure 10(c)). All specimens contain notches that are sharpened with fatigue cracks [6].

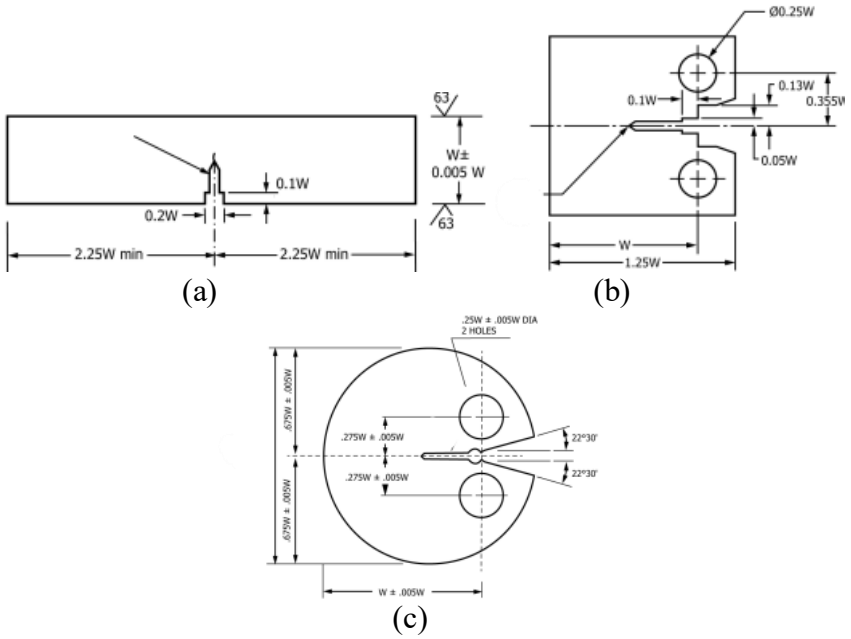

Figure 10. Examples of the different shapes of the metal specimens

The procedure to follow is to load the sample in steps with displacements gradually increasing. Between each step a partial unloading is performed to determine the compliance C, as shown in Figure 11 (a given unload must not fall below 50% of the previous load).

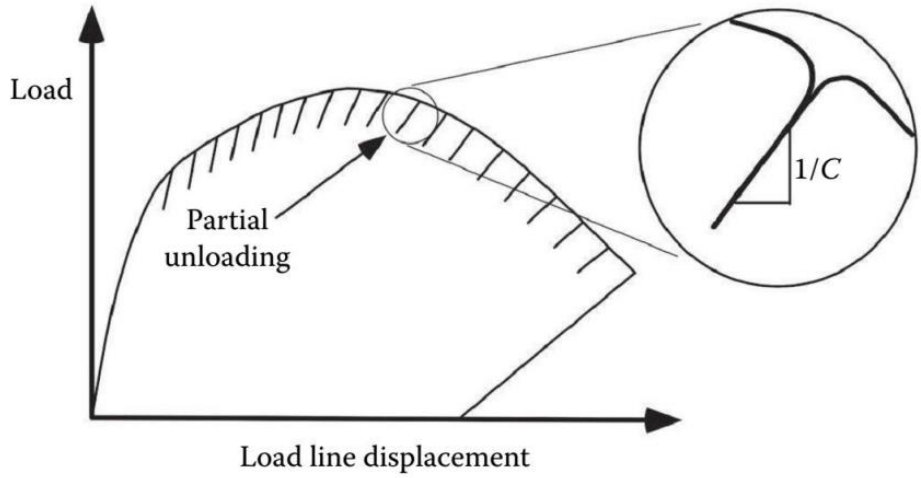

Figure 11. Procedure of the load and unload steps

The compliance is measured to estimate the original crack size, a_o, using unloading/reloading sequences over a force range of 0.5 to 1.0 times the final maximum precracking force. Then, it is estimated the provisional initial crack size, a_{oq}, from at least three unloading/reloading sequences [6].

The maximum recommended range of unload/reload for crack extension measurement should not exceed either 50 % of Pm, or 50 % of the current force, whichever is smaller. Experience has shown that satisfactory results may be obtained with unloads of 10-20% of Pm [6]. A consistent force range should be used for all unloadings in the test.

A minimum of twenty (crack opening displacement, force) data points, uniformly spaced over the unload interval, are required to estimate the specimen compliance. The uncertainty of the compliance estimates can be improved by increasing the number of data points used in the regression analysis. It is recommended that forty or more data points be used in the regression analysis of each unload (reload) [6].

For each unload it is calculated the point J-Δa. The simplest method would be:

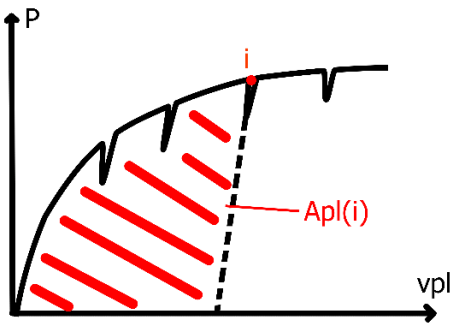

Figure 12. Integration area of point i

For each ai value, it is calculated a corresponding Δai as follows:

$$\Delta a_i = a_i - a_{0q} \qquad \text{Eq. 14}$$

From which it would be obtained a series of data $J^i - \Delta a^i$. However, it is preferable to carry out a calculation more precise. In fact, the formula:

$$J = J_{el} + J_{pl} = \frac{K_I^2}{E'} + \eta \frac{1}{B b_0} A_{pl} \qquad \text{Eq. 15}$$

was originally demonstrated for the case of a crack whose crack length 'a' remains constant during load application, while in this case 'a' generally increases.

An example of the loading path of each step can be seen in Figure 13.

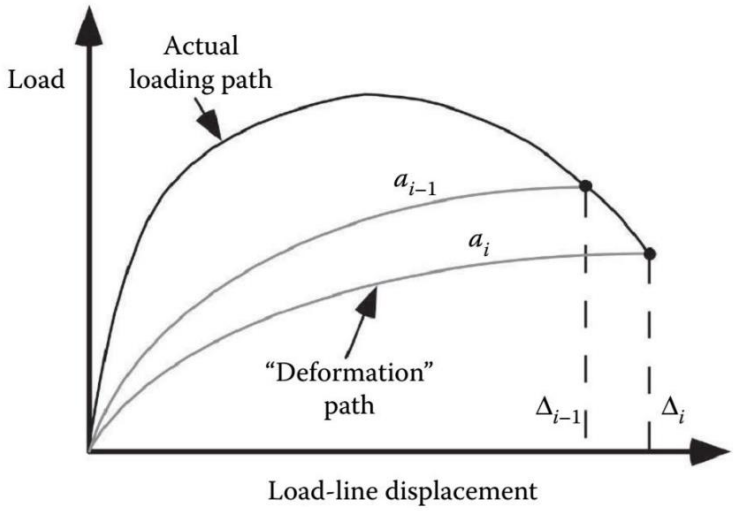

Figure 13. Loading and deformation path of load step a_i

From this it is considered using an incremental formula – i.e. J^i is calculated starting from J^{i-1} by applying a formula that takes into account both the increase in the plastic area from the step i to the step i+1 and a correction factor based on the increase in crack length between the same steps.

J_Q is determined from the curve J-Δa as seen in Figure 14.

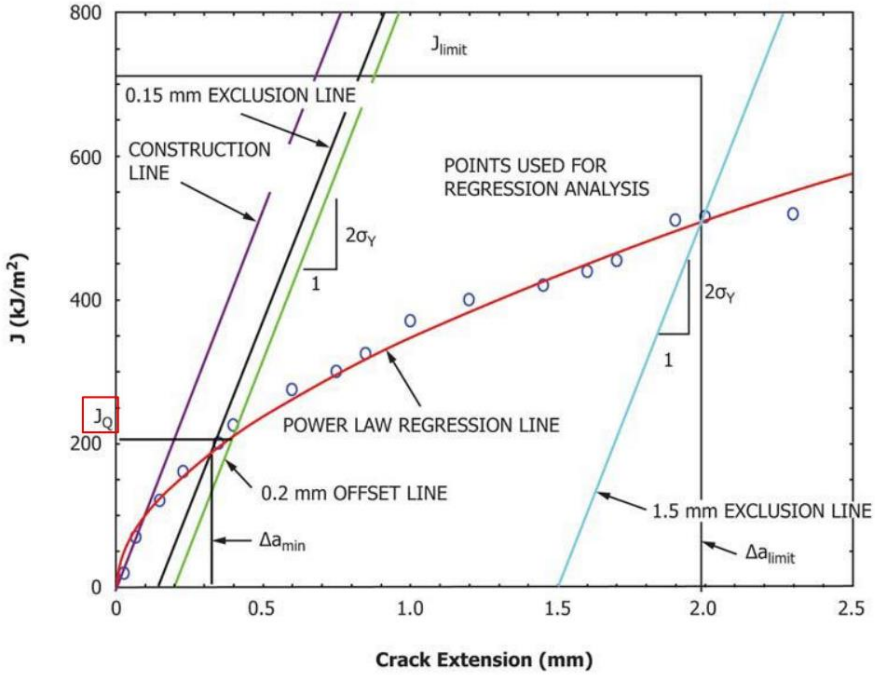

Figure 14. J_Q calculation from the curve J-Δa (crack extension)

J_Q is defined as the transition point between the tip blunting and the plastic tearing. During the initial rounding phase of the apex, J presents approximately linear trend with respect to Δa. The initial slope, however, is difficult to estimate, because the graph has few points; therefore, it is preferred to assume by hypothesis that the initial slope = 2 σ_y (with σ_y=yield stress) –see "construction line" in Figure 14 (This is because in the rounding phase Δa is proportional to δ (deformation), which in turn is proportional to J).

When plastic tearing occurs, however, Δa increases significantly more rapidly than J. Therefore, the curve has a point of transition. To determine this point, a conventional geometric construction is used (very similar to the one used to determine the conventional yield strength in a tensile curve). A reference line ("0.2 mm offset line") is drawn parallel to the construction line, but shifted by 0.2 mm. The J_Q is defined as the intersection between this straight line and the J - Δa curve.

Unfortunately, it often happens that the J – Δa curve is made up of just a few experimental points, with high noise; reason why the point of intersection is uncertain. To avoid this problem, all experimental points which fall within a certain distance are selected, in practice between the two "exclusion lines" in Figure 14) and a function of interpolation is applied to them; then it is found the intersection between the reference line and the interpolating function.

Finally, before confirming $J_{Ic} = J_Q$, it must be verified:

- if the pre-cracking was carried out in an "adequate" manner with respect to the final results and whether the precrack (which can be observed after breaking the sample) is "fairly" regular.

- if the initial and final crack lengths (which are measured after the test, having marked and broken the sample) are “not too much” different from the estimates obtained with the compliance method.

-if the measurement points in the J – Δa plane are “fairly” numerous and
“fairly” well distributed.

- if the sample size is adequate, i.e. if:

$$\text{Thickness, } B > 10\, J_Q / \sigma_Y,$$

$$\text{Initial ligament, } b_o > 10\, J_Q / \sigma_Y,$$

The fracture toughness test is carried out with the same machine used for traction tests, but the appropriate instrumentation has been mounted which allows to carry out the fracture toughness tests on three points as shown in Figure 15.

3.2. Experimental setup

In Figure 15 it is seen the preparation of the test. It is highlighted the positioning of the camera and the Lamp used to acquire the images necessary for DIC analysis. It is also seen the 3 load points, being the middle one used to apply the Force.

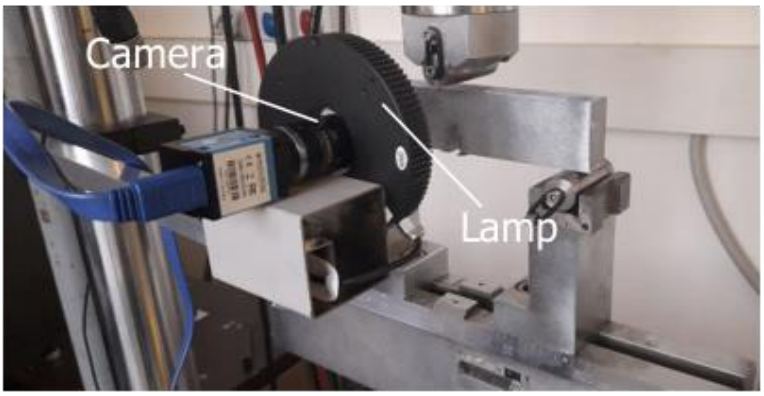

Figure 15. Machine for carrying out fracture toughness tests [1]

In the Figure 16 is seen the fracture toughness testing machine with one of the specimens used for testing.

There were added two metal plates in the external part of the opening with the function of acting as a grip for the mechanical strain gauge. The following image, Figure 16, is inserted to clarify how the strain gauge was inserted.

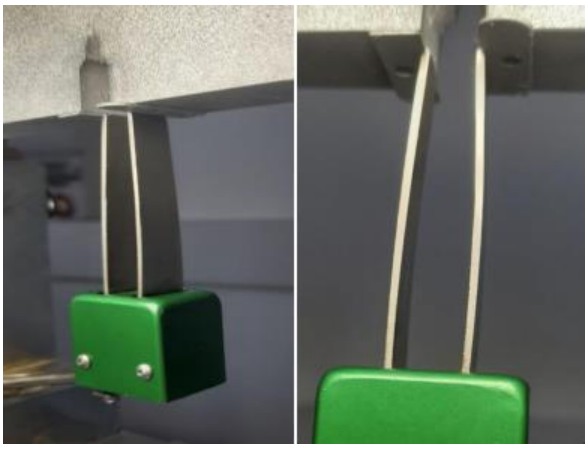

Figure 16. Positioning of mechanical strain gauge with metal plates [1]

It is also seen the speckle pattern applied to the specimen with paint, in order to create a reference for DIC analysis.

The two metal plates were glued and during insertion of the strain gauge, particular attention was paid not to create impacts that could cause damage the detachment.

3.3. Test material

The specimen subjected to three-point fracture toughness test is made of steel $39NiCrMo3$ [1] which is one of the most used hardened and tempered steels in Italy.

The mechanical characteristics of the material were taken from an article published by Roberti, La Vecchia and Firrao [7]. The specimens were obtained in the longitudinal direction with respect to the processing of the material from which they were obtained. In this case the tempering was carried out at a temperature of $600°C$.

After preparing the sample 44, it is observed under an optical microscope. An image was acquired for both magnification 20 and one with magnification 100 (see Figure 17).

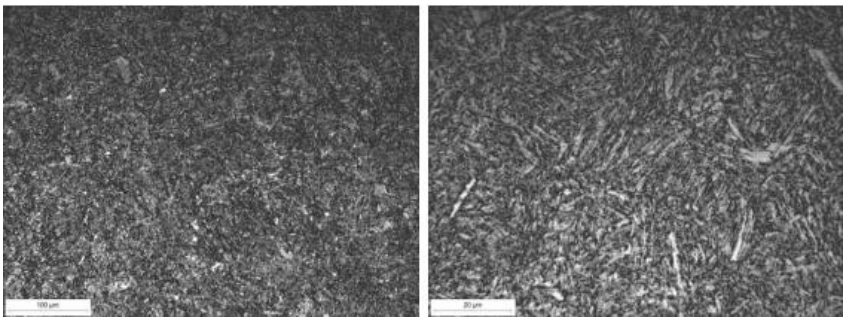

Figure 17. Images acquired with an optical microscope of Test 44, on the left magnification 20, on the right magnification 100 [1]

3.4. Test specimen

In terms of the dimensions of the sample, as can be seen in Figure 18 and Table 1, 'W' is taken as the vertical width of the sample, while 'B' is the horizontal width.

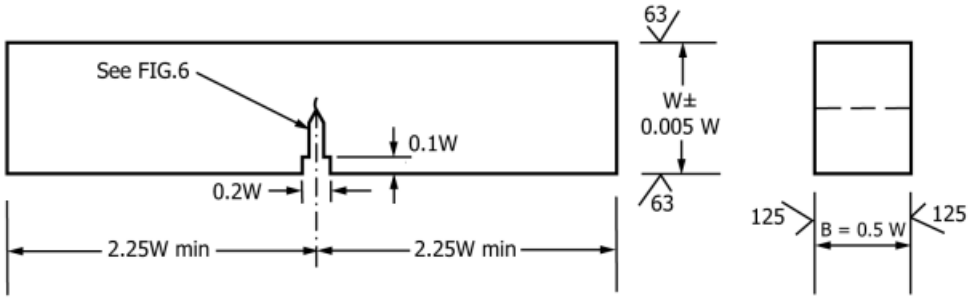

NOTE 1—The two side planes and the two edge planes shall be parallel and perpendicular as applicable to within 0.5°.
NOTE 2—The machined notch shall be perpendicular to specimen length and thickness to within ±2°.

Figure 18. General dimensions of the sample

The Flow stress value is approximated as an intermediate value between Yield Strength and Ultimate Tensile Strength.

S: Length of the sample

σ_y: Flow stress

YS: Yield Strength

E: Elastic Modulus

UTS: Ultimate Tensile Strength

v: Poisson Modulus

W	B	S	YS	UTS	σ_y	E	v
mm	mm	mm	MPa	MPa	MPa	GPa	-
40	20	160	922	1049	985.5	200	0.3

Table 1. Geometrical data of the sample

3.5. Test procedure

On the following Table is indicated the first part of the load and unload experiment (the absolute values). A total of 9758 data points were measured, recording the load and displacement of each data point. With the value of Force indicated in [N] and the displacement in [mm].

	|Force|	|Displ|
1	260.89	0.0006
2	261.52	0.00083
3	259.59	-0.00059
4	259.89	0.00037
5	262.43	0.00112
6	261.45	-0.0005
7	262.89	0.00097
8	262.56	0.00024
9	268.79	0.00026
10	272.22	-0.00035
11	274.46	0.00094
12	276.38	0.00033
13	285.06	0.00133

Table 2. First 13 Timesteps of the Measured Load and Displacement

In total there were carried out 67 load and reload steps during the experiment, as can be seen in part in Table 3.

Num. unload	start unload [s]	start load [s]
1	9	12
2	17	19
3	24	26
4	31	34
5	39	41
6	45	48
7	53	55
8	60	63
9	68	70
10	75	77
11	82	85
12	90	92
13	97	99
14	105	107
15	113	115
16	121	123
17	129	131
18	137	140
19	146	148
20	154	156

Table 3. Time in seconds of the first 20 unload steps

The Force-Displacement graph of the test is depicted in Figure 19.

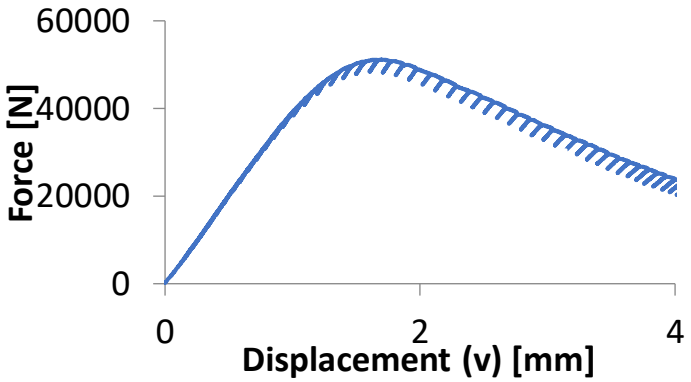

Figure 19. Displacement vs Force result of unload/reload test 44

Table 4 indicates some of the results of the 67 Unload steps. The 2nd and 3rd column represent the maximum force applied and the measured extensometer opening before the i-th unload starts (the negative sign just indicates the Force exerted downwards). The 4th column represents the compliance (with respect to the COD). The 5th column represents the crack opening displacement (COD or v) and equals the present extensometer opening minus the initial extensometer opening.

Num unload	P [N]	Extensometer Opening [mm]	Compliance (C) [µm/kN]	v [mm]
1	-7,953535e+03	2,971740e+00	-1,142345e-05	0.085
2	-1,045384e+04	2,999296e+00	-1,116263e-05	0.113
3	-1,296071e+04	3,027226e+00	-1,115630e-05	0.141
4	-1,546601e+04	3,055856e+00	-1,133597e-05	0.169
5	-1,792357e+04	3,083786e+00	-1,104877e-05	0.197
. . .				
30	-3,989742e+04	4,744143e+00	-1,884764e-05	1.858
31	-3,851512e+04	4,841188e+00	-1,948120e-05	1.955
32	-3,727999e+04	4,936697e+00	-1,892189e-05	2.050
. . .				
64	-1,620112e+04	7,758530e+00	0,000000e+00	4.872
65	-1,595948e+04	7,758530e+00	0,000000e+00	4.872
66	-1,575773e+04	7,758530e+00	0,000000e+00	4.872
67	-1,551293e+04	7,758530e+00	0,000000e+00	4.872

Table 4. Unload steps

To organize the calculations, the first part (first four columns) of the Table 5 contains the experimental data measured.

i : Represents the number of the unload step

P: Force before the i-th unloading in kN

v: Displacement before the i-th unloading in mm

C: compliance (slope of the curve) of the i-th unload in μm/kN

The 5th to the 8th columns of Table 5 are used to calculate the crack size. For a resistance curve test method using an elastic compliance technique on single edge bend specimens with crack mouth opening displacements measured at the notched edge, the crack size is given as follows:

$$\frac{a_i}{W} = [0.999748 - 3.9504u + 2.9821u^2 - 3.21408u^3 + 51.51564u^4 - 113.031u^5]$$

Eq. 16

Where:

$$u = \frac{1}{\left[\frac{B_e WEC_i}{S/4}\right]^{1/2} + 1}$$

Eq. 17

For the estimation of 'b' it is taken into account the relation:

$$W = a + b$$

Eq. 18

The 9th to 11th columns of Table 5 are used to calculate K and J_{el}. For the compact specimen at a force P(i), K is calculated as follows:

$$K_{(i)} = \frac{P_{(i)}}{B\sqrt{W}} f\left(\frac{a_i}{W}\right)$$

Eq. 19

With

$$f\left(\frac{a_i}{W}\right) = \frac{3\left(\frac{a_i}{W}\right)^{1/2}\left[1.99 - \left(\frac{a_i}{W}\right)\left(1 - \frac{a_i}{W}\right)\left(2.15 - 3.93\left(\frac{a_i}{W}\right) + 2.7\left(\frac{a_i}{W}\right)^2\right)\right]}{2\left(1 + 2\frac{a_i}{W}\right)\left(1 - \frac{a_i}{W}\right)^{3/2}}$$

Eq. 20

$$J_{(i)} = \frac{\left(K_{(i)}\right)^2 \left(1 - \nu^2\right)}{E} + J_{pl(i)}$$

Eq. 21

The 12th and 13th columns are then used to estimate the plastic deformation and plastic work.

$V_{pl(i)}$ = plastic part of the load-line displacement, $v_i - P_{(i)}C_{LL(i)}$ (see Figure 20).

$C_{LL(i)}$ = experimental compliance, $(\Delta v/\Delta P)_i$, corresponding to the current crack size, a_i (Used in this case the C value previously computed)

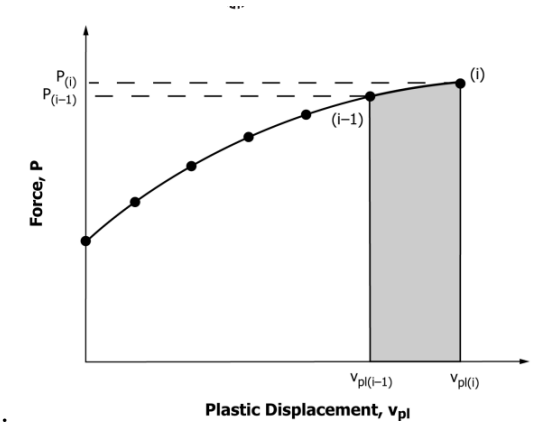

Figure 20. Definition of Plastic Area for Resistance Curve. J Calculation

And

$$A_{pl(i)} = A_{pl(i-1)} + \left[P_{(i)} + P_{(i-1)}\right]\left[v_{pl(i)} - v_{pl(i-1)}\right]/2 \qquad \text{Eq. 22}$$

The quantity $A_{pl(i)} - A_{pl(i-1)}$ is the increment of plastic area under the chosen force versus plastic displacement record between lines of constant plastic displacement at points i−1 and i. The quantity $J_{pl(i)}$ represents the total crack growth corrected plastic J at point i and is obtained in two steps by first incrementing the existing $J_{pl(i-1)}$ and then by modifying the total accumulated result to account for the crack growth increment [6].

Columns 14th to 16th of Table 5 are used to calculate the plastic component of J, with the correction factors η_{pl} and γ_{pl} that take into account the effect of the crack growth.

$$J_{pl(i)} = \left[J_{pl(i-1)} + \left(\frac{\eta_{pl(i-1)}}{b_{(i-1)}}\right)\left(\frac{A_{pl(i)} - A_{pl(i-1)}}{B_N}\right)\right] \times \left[1 - \gamma_{pl(i-1)}\left(\frac{a_{(i)} - a_{(i-1)}}{b_{(i-1)}}\right)\right] \qquad \text{Eq. 23}$$

$$\eta_{pl} = 3.667 - 2.199\left(\frac{a_{(i-1)}}{W}\right) + 0.437\left(\frac{a_{(i-1)}}{W}\right)^2 \qquad \text{Eq. 24}$$

$$\gamma_{pl} = 0.131 + 2.131\left(\frac{a_{(i-1)}}{W}\right) - 1.465\left(\frac{a_{(i-1)}}{W}\right)^2 \qquad \text{Eq. 25}$$

Experimental data				Calcoli												J-Δa Curve		Interp. Curve	
i	**P**	**v**	**C**	**u**	**a/W**	**a**	**b**	**f**	**K**	**J_{el}**	**v_{pl}**	**A_{pl}**	**η_{pl}**	**γ_{pl}**	**J_{pl}**	**J**	**Δa**	a (int)	J (int)
-	kN	mm	µm/kN	-	-	mm	mm	-	MPa√m	kJ/m^2	mm	J	-	-	kJ/m^2	**kJ/m^2**	**mm**	mm	kJ/m^2
start	0				0.54	21.6	18.4				0	0	2.61	0.854	0	**0**		21.55275	
1	8.0	0.09	11.42	0.129	0.54	21.7	18.3	3.07	24.4	2.7	-0.01	0.0	2.60	0.856	-0.2	**2.6**	**0.19**	21.55	
2	10.5	0.11	11.16	0.130	0.54	21.6	18.4	3.03	31.7	4.6	0.00	0.0	2.61	0.854	0.0	**4.5**	**0.03**	21.55	
3	13.0	0.14	11.16	0.130	0.54	21.6	18.4	3.03	39.3	7.0	0.00	0.0	2.61	0.854	0.0	**7.0**	**0.02**	21.56	
4	15.5	0.17	11.34	0.129	0.54	21.7	18.3	3.06	47.3	10.2	-0.01	0.0	2.60	0.856	-0.3	**9.9**	**0.13**	21.56	
5	17.9	0.20	11.05	0.131	0.54	21.5	18.5	3.01	54.0	13.3	0.00	0.1	2.61	0.853	0.4	**13.6**	**-0.04**	21.56	
6	20.4	0.23	11.04	0.131	0.54	21.5	18.5	3.01	61.6	17.2	0.00	0.1	2.61	0.853	0.6	**17.8**	**-0.05**	21.56	
7	23.0	0.26	11.01	0.131	0.54	21.5	18.5	3.01	69.1	21.7	0.00	0.1	2.61	0.853	1.0	**22.7**	**-0.07**	21.56	
8	25.4	0.29	11.00	0.131	0.54	21.5	18.5	3.01	76.5	26.6	0.01	0.2	2.61	0.853	1.5	**28.1**	**-0.07**	21.56	
9	28.0	0.32	11.16	0.130	0.54	21.6	18.4	3.03	84.8	32.7	0.01	0.2	2.61	0.854	1.3	**34.0**	**0.03**	21.56	
10	30.4	0.35	10.97	0.131	0.54	21.5	18.5	3.00	91.3	38.0	0.02	0.5	2.61	0.853	3.5	**41.4**	**-0.09**	21.56	
11	32.9	0.38	11.17	0.130	0.54	21.6	18.4	3.03	99.9	45.4	0.02	0.5	2.61	0.854	3.4	**48.8**	**0.03**	21.55	
12	35.4	0.42	10.98	0.131	0.54	21.5	18.5	3.00	106.4	51.5	0.03	1.0	2.61	0.853	6.9	**58.4**	**-0.09**	21.55	
13	38.0	0.46	11.19	0.130	0.54	21.6	18.4	3.04	115.3	60.5	0.03	1.1	2.61	0.855	7.8	**68.3**	**0.05**	21.56	
14	40.5	0.50	11.00	0.131	0.54	21.5	18.5	3.00	121.6	67.2	0.06	2.0	2.61	0.853	14.4	**81.6**	**-0.08**	21.56	
15	43.0	0.55	11.01	0.131	0.54	21.5	18.5	3.01	129.1	75.9	0.08	3.0	2.61	0.853	21.2	**97.1**	**-0.07**	21.58	
16	45.4	0.61	11.38	0.129	0.54	21.7	18.3	3.07	139.2	88.1	0.10	3.8	2.60	0.856	26.4	**114.5**	**0.16**	21.61	
17	47.5	0.68	11.43	0.129	0.54	21.7	18.3	3.07	145.9	96.8	0.14	5.7	2.60	0.857	39.9	**136.8**	**0.19**	21.68	
18	49.0	0.75	11.49	0.129	0.54	21.8	18.2	3.08	151.1	103.9	0.19	8.1	2.60	0.857	56.9	**160.9**	**0.23**	21.81	152
19	50.0	0.83	11.92	0.127	0.55	22.0	18.0	3.15	157.6	113.1	0.23	10.1	2.59	0.860	70.7	**183.8**	**0.48**	21.99	199
20	50.5	0.91	12.28	0.125	0.56	22.2	17.8	3.21	161.9	119.3	0.29	13.0	2.58	0.863	90.6	**209.8**	**0.68**	22.27	226
21	50.3	0.99	12.33	0.125	0.56	22.3	17.7	3.21	161.7	118.9	0.37	17.4	2.58	0.863	122.1	**241.0**	**0.71**		230
22	49.7	1.09	12.96	0.122	0.56	22.6	17.4	3.31	164.5	123.1	0.44	20.7	2.56	0.867	144.2	**267.3**	**1.04**		264
23	48.7	1.18	13.41	0.120	0.57	22.8	17.2	3.38	164.5	123.1	0.53	25.0	2.55	0.870	173.3	**296.4**	**1.27**		284
24	47.5	1.28	14.46	0.116	0.58	23.3	16.7	3.54	167.8	128.2	0.59	28.1	2.53	0.875	191.8	**320.0**	**1.76**		320
25	46.2	1.38	14.63	0.116	0.58	23.4	16.6	3.56	164.6	123.2	0.70	33.1	2.53	0.876	229.0	**352.2**	**1.84**		
26	44.8	1.48	15.15	0.114	0.59	23.6	16.4	3.64	163.0	120.9	0.80	37.6	2.52	0.878	259.7	**380.6**	**2.06**		
27	43.6	1.57	16.05	0.111	0.60	24.0	16.0	3.77	164.1	122.5	0.88	41.0	2.51	0.882	280.7	**403.2**	**2.43**		
28	42.4	1.67	16.28	0.110	0.60	24.1	15.9	3.80	160.9	117.8	0.98	45.3	2.50	0.883	312.8	**430.6**	**2.52**		
29	41.2	1.76	16.78	0.109	0.61	24.3	15.7	3.87	159.3	115.4	1.07	49.2	2.49	0.885	339.3	**454.8**	**2.71**		
30	39.9	1.86	18.85	0.103	0.62	25.0	15.0	4.16	165.9	125.2	1.11	50.7	2.46	0.890	337.3	**462.5**	**3.43**		
31	38.5	1.95	19.48	0.102	0.63	25.2	14.8	4.24	163.4	121.5	1.20	54.6	2.46	0.892	364.7	**486.2**	**3.63**		
32	37.3	2.05	18.92	0.103	0.63	25.0	15.0	4.17	155.4	109.8	1.34	59.9	2.46	0.891	413.1	**522.9**	**3.45**		
33	35.9	2.14	19.31	0.102	0.63	25.1	14.9	4.22	151.7	104.7	1.45	63.6	2.46	0.892	440.6	**545.3**	**3.58**		
34	35.0	2.23	35.74	0.077	0.71	28.5	11.5	6.25	218.5	217.1	0.98	47.2	2.32	0.906	243.2	**460.4**	**6.95**		
35	33.7	2.33	21.60	0.097	0.64	25.8	14.2	4.53	152.5	105.8	1.60	68.5	2.43	0.896	555.8	**661.6**	**4.24**		
36	32.6	2.42	21.24	0.098	0.64	25.7	14.3	4.48	145.8	96.7	1.73	72.6	2.43	0.895	595.0	**691.7**	**4.14**		
37	31.6	2.51	22.12	0.096	0.65	25.9	14.1	4.59	145.1	95.8	1.81	75.3	2.43	0.897	608.2	**704.0**	**4.38**		
38	30.5	2.60	22.71	0.095	0.65	26.1	13.9	4.67	142.4	92.2	1.90	78.2	2.42	0.898	626.9	**719.2**	**4.53**		
39	29.5	2.68	24.72	0.091	0.66	26.6	13.4	4.93	145.3	96.0	1.95	79.7	2.40	0.900	620.4	**716.5**	**5.01**		
40	28.4	2.77	24.99	0.091	0.67	26.6	13.4	4.96	140.9	90.3	2.06	82.8	2.40	0.900	645.8	**736.1**	**5.07**		
41	27.4	2.86	25.62	0.090	0.67	26.8	13.2	5.04	138.3	87.0	2.15	85.4	2.39	0.901	662.4	**749.4**	**5.21**		
42	26.6	2.94	26.30	0.089	0.67	26.9	13.1	5.12	136.1	84.2	2.24	87.7	2.39	0.902	676.5	**760.7**	**5.35**		
43	25.8	3.01	27.15	0.088	0.68	27.1	12.9	5.23	134.9	82.8	2.31	89.6	2.38	0.902	685.3	**768.1**	**5.53**		
44	24.9	3.08	27.89	0.086	0.68	27.2	12.8	5.32	132.6	80.0	2.39	91.4	2.37	0.903	695.5	**775.6**	**5.67**		
45	24.3	3.16	29.17	0.085	0.69	27.5	12.5	5.48	133.0	80.5	2.45	93.0	2.36	0.904	697.8	**778.3**	**5.91**		
46	23.5	3.23	29.72	0.084	0.69	27.6	12.4	5.54	130.4	77.4	2.53	95.0	2.36	0.904	711.4	**788.8**	**6.01**		
47	22.9	3.29	30.40	0.083	0.69	27.7	12.3	5.62	129.0	75.7	2.60	96.5	2.35	0.904	719.6	**795.3**	**6.13**		

Table 5. Calculation results of Test 44

The J-a curve is interpolated with the following formula in order to obtain the a_0 or initial crack length

$$a = a_{0q} + \frac{J}{2\sigma_Y} + BJ^2 + CJ^3 \qquad \text{Eq. 26}$$

The results previously calculated are depicted in Figure 21, where the J-a points obtained are plotted and interpolated in order to obtain the a_{0q} point.

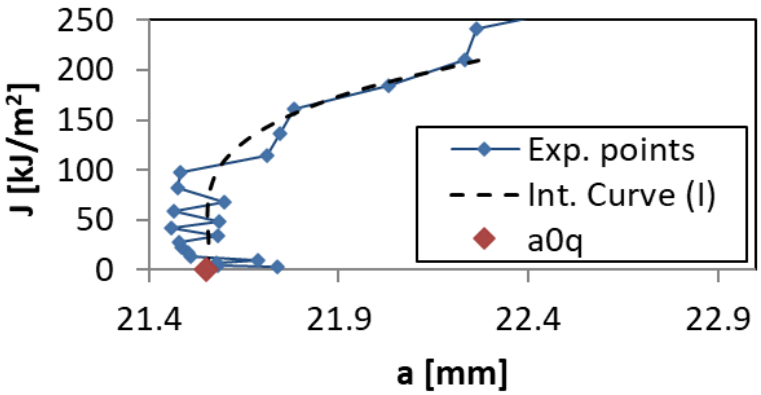

Figure 21. J-a curve

In Table 6 are represented the interpolation values.

Interp. per a_{0q}		
C	**B**	**a_{0q}**
1.5E-07	-1.7E-05	2.2E+01

Table 6. Interpolation of J-a curve

After substracting a_0, the J-a curve is obtained and interpolated using Eq. 27, considering just the points J_C between the two exclusion lines with offset 0.15 and 1.5 mm. The results of this interpolation is shown in Table 7.

$$J = C1(\Delta a/k)^{C2} \qquad \text{Eq. 27}$$

Interp. per J_{Ic}		
C_1	**C_2**	**Ln(C_1)**
260.5	**0.364**	5.56

Table 7. Interpolation for J_{IC}

In Table 8 are constructed the exclusion Lines that are taken into account in the analysis (1st column for the 1st exclusion line with offset of 0.15 [mm] and 3rd column for the 2nd exclusion line with offset of 1.5 [mm]) and the construction line with offset of 0.2 [mm] (2nd column), while last two columns are used to establish boundaries for calculation.

Inclinated lines				sup. Limit	
J	Δa	Δa	Δa	J	Δa
kJ/m²	mm	mm	mm	kJ/m²	mm
0	0.15	0.2	1.5	112	0
1500	0.91	0.96	2.26	112	4

Table 8. Exclusion and construction lines definition

J_{Ic} is obtained as the intersection between the interpolating curve and the line of construction with offset 0.2 mm (the intersection point is calculated in iterative way as seen in Table 9).

Calculus of J_{Ic}	
Δa	**J**
mm	**kJ/m^2**
0.281614	160.861
0.283324	164.232
0.283508	164.595
0.283528	164.633
0.283530	164.638
0.283530	164.638
0.283530	164.638
J_{Ic}	**164.6**

Table 9. Iterative calculation of J_{IC}

In Figure 22 is replicated the procedure previously detailed in order to obtain the interpolated value J_{IC}.

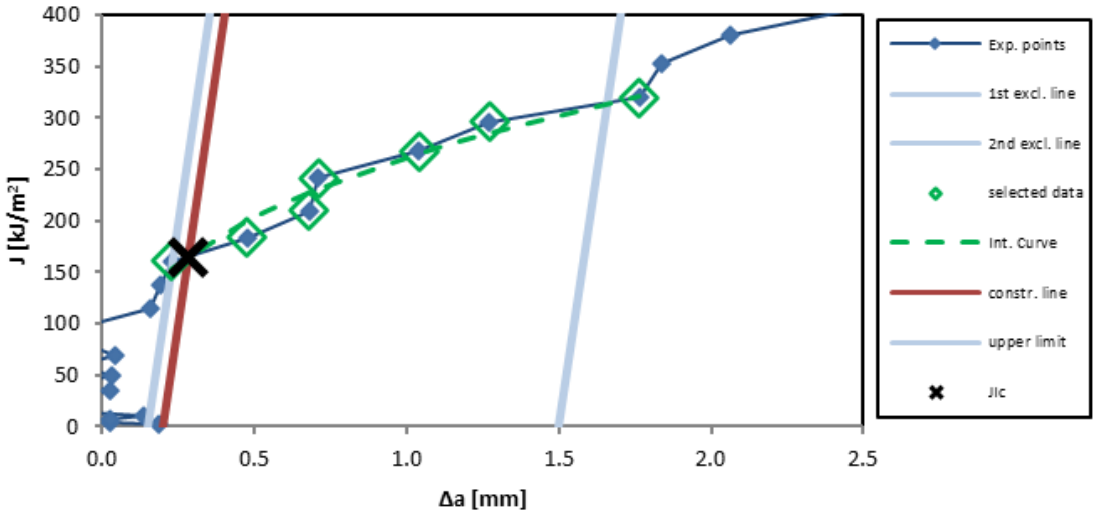

Figure 22. J-Δa curve

4. Digital Image Correlation

This chapter delves into the fundamental principles, methodology, and practical considerations of DIC, highlighting its application in the analysis of fracture mechanics, particularly in the calculation of the J-integral.

Digital Image Correlation (DIC) is a powerful optical method used for measuring full-field displacements and strains on the surface of a specimen under deformation. It has gained significant relevance in experimental mechanics due to its non-contact nature, high spatial resolution, and ability to capture complex deformation patterns. The process includes image acquisition, preprocessing, identifying patterns or markers, analyzing deformation, and post-processing and visualization.

To measure how an object changes shape and moves, a camera or group of cameras take high-quality images before and after the change occurs. These images go through different processing techniques to improve their quality and reduce any unwanted effects that could interfere with tracking.

Some common materials that are tested include metals, polymers, concrete, geological samples, biological tissues, battery electrodes, explosives, etc. and test pieces range from, for example, small coupons used in tensile tests up to entire sub-assemblies of aircraft. This versatility has led to a plethora of methodologies and software codes, both commercial and independently developed, to utilize the data captured from a DIC measurement. Digital image correlation is especially helpful for studying mechanical properties and complicated deformations and getting detailed strain information. DIC is commonly employed in experimental mechanics and materials science to obtain accurate and reliable measurement data for mechanical properties and beyond [8].

In the mechanical engineering field, digital image correlation has been widely used to monitor and process test data in both research and industrial contexts, for applications ranging from common material testing to characterization of massive and complex components (part of an airplane or a helicopter, roadway bridges, nuclear power-plant structures). The method is very versatile and can be applied indifferently to structures of any shape, size, or material, as long as they can be observed by cameras. It is also a contactless and non-destructive technique [8].

At the core level, DIC estimates full-field coordinates and displacements from a sequence of digital images taken of a pattern on the surface of a test piece, by solving an optimization problem, typically based on a transport model such as optical flow. A fundamental assumption in DIC measurements is that the pattern on the surface of the test piece, either natural or applied, follows the deformation of the underlying test piece. Thus, the images of the test piece taken throughout the test can be correlated to produce full-field coordinates representative of the shape, motion and deformation of the surface of the test piece (see Figure 23). 2D coordinates of the surface can be measured using a single camera system, and this is referred to as 2D-DIC [9].

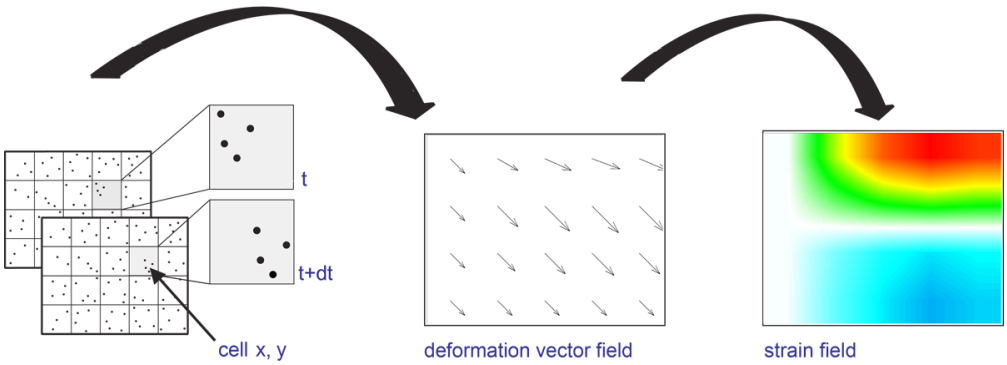

Figure 23. Digital Image correlation calculation logic

Comparing the positions of these markers helps the software calculate the displacement and strain fields, which reveal important information about localized strain distributions.

In brief, a software code analyzes a user-defined region-of-interest (ROI) within the images, which contains a set of interrogation, or measurement, points. In local DIC, each interrogation point is centered within a subset of the image. The interrogation points are typically defined at some regular spacing (step size), such that neighboring subsets may (or may not) overlap. The subsets are numerically correlated from the reference image (before motion/deformation) to each subsequent image (during motion/deformation). This correlation is performed by first approximating the pattern in each subset using an interpolant function, and then allowing that function to deform from the reference image based on a subset shape function. A matching criterion in conjunction with subset weights is used to match each subset in the reference image with the corresponding subset in the deformed images [9].

Just like the human eye, a digital image correlation algorithm must be able to determine the displacement (i.e., rigid body motion that is a combination of rotation and translation) and deformation of a pattern across several images:

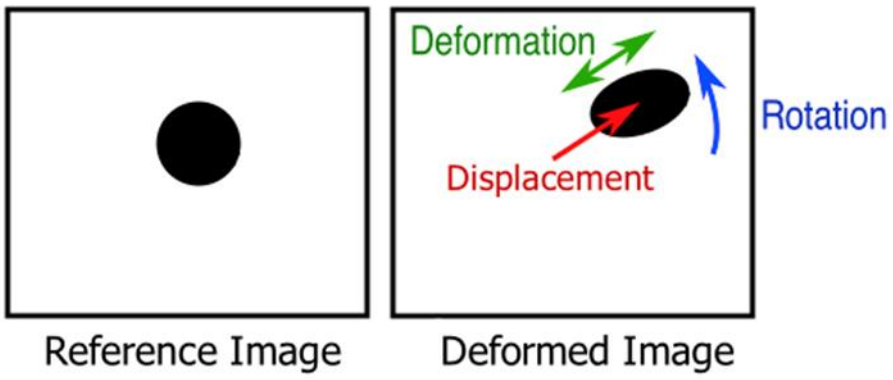

Figure 24. DIC variables to compare reference vs deformed image [8]

Conversely, ‘periodic’ texture patterns should be avoided because it will become difficult for the digital image correlation software to determine individual point locations unequivocally (see Figure 25 as a reference).

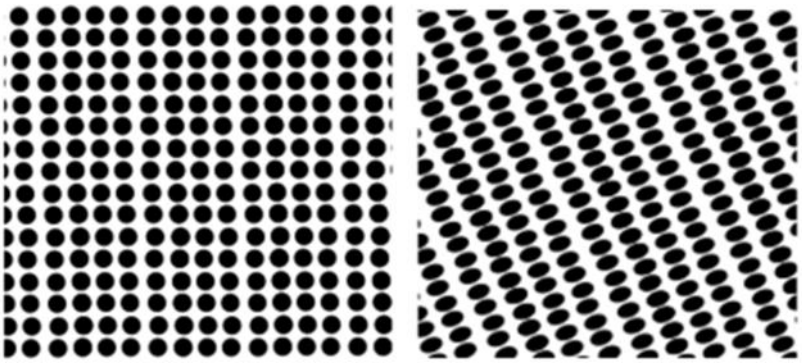

Figure 25. Speckles uniform pattern to be avoided in DIC [8]

To remove this ambiguity on individual point locations for digital image correlation, a random texture that allows to distinguish the vicinity of a given point from the surrounding areas is preferred (see Figure 26 as a reference). For parts with sizes ranging from a centimeter up to a meter, paint speckle patterns are often directly sprayed on the sample surface. The resulting texture is made of randomly distributed speckles of 1mm in average diameter [8].

Every measurement point (in practice, every image ‘subset’) can then be distinguished from its surroundings. Acceptable textures for DIC can be obtained from other methods, for imaging techniques ranging from Secondary Electron Microscopy (SEM) and X-Ray tomography up to observations of much larger structures [8].

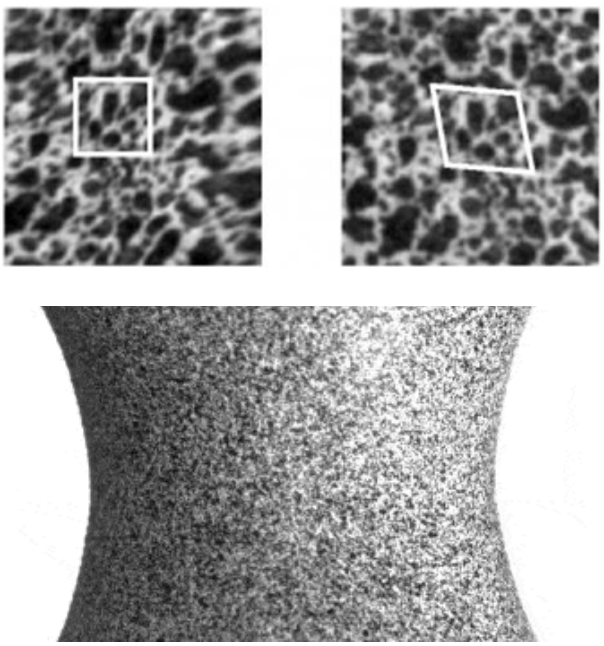

Figure 26. Example of speckles pattern on a test piece [8]

Both natural and applied patterns should have the following general characteristics:

- **Size**

The optimum pattern feature size is 3–5 pixels.

- **Variation**

The pattern should have sufficient random variation such that subsets in different regions of the image can be uniquely identified.

- **Density**

Pattern density should be approximately 50 % (i.e. there should be approximately the same area of light (white) and dark (black) pixels in any intended subset of the ROI of the image). If round speckles are used, then a density closer to 25–40 % can be expected due to the required minimum spacing between the round speckles.

- **Quality**

Pattern quality degradation should be minimized and not permitted to result in decorrelation during the analysis.

- **Reflections**

The pattern sheen should be matte and not glossy, to avoid glare and specular reflections.

Applied patterns, regardless of the method used to create them (i.e. painting, applying an adhesive-backed foil or sticker, stamping, or drawing with ink, applying a powder, transfer printing, etc.), should have the following additional characteristics, which do not necessarily apply to natural patterns.

- **Compliance**

The applied pattern should be thin and compliant relative to the test piece, such that it does not change the test piece behavior being measured during the test.

- **Bonding**

There should be good bonding between the test piece and the applied pattern.

- **Fidelity**

The applied pattern should move and deform conformally with the test piece surface.

- **Thickness**

The pattern should be of uniform thickness. The calculation of derived field quantities is the final step in many DIC processing schemes.

The most derived quantities from these coordinate fields are probably strains, though DIC provides access to other quantities of interest, such as curvature, velocity and acceleration. The minimum resolution (also called the noise-floor) of the quantities of interest, as well as potential bias errors, are tied to both the measurement setup (e.g. camera selection, image contrast, DIC pattern feature size), and the data processing parameters (e.g. subset size, subset shape function, virtual strain gauge). Therefore, determination of the resolution of the quantities of interest through uncertainty quantification analysis completes the DIC data processing. This leaves the user with a full-field description of displacements, and/or derived quantities, of a test piece subjected to a mechanical test, as well as the uncertainties of those measurements [9].

Typically, the regions of interest of the test piece should almost fill the field of view to optimize the spatial resolution, while still remaining in the field of view throughout the test.

One fundamental assumption of DIC is that the motion and deformation of the pattern that is imaged exactly replicates the underlying test piece motion and deformation. Sometimes, images of the surface of the test piece itself have a sufficient natural pattern that is adequate for DIC, and no artificial pattern needs to be applied [9].

The digital image correlation software can then extract relevant data and present it visually by using techniques like contour plots or animations.

The measurement accuracy of digital image correlation can seem surprisingly high. It is due to sub-pixel grey level interpolation: if a black spot with a diameter of 1 pixel is translated across a uniform white background, the neighboring pixels will react to this displacement by taking a grey level value proportional to the surface of the dot overlapping this pixel. Sub-pixel interpolation makes it possible to commonly measure displacement amplitudes smaller than 0.1 pixel, and even smaller than 0.01 pixel in favorable experimental conditions. To achieve this precision, great care must be taken in providing constant and uniform lighting to the observed sample, and image acquisition must be carried out with high-quality lenses and cameras [8].

5. DIC Analysis

A total of 615 images were taken during the test with a frequency of 1 [Hz] (so 1 image is taken per second). The initial condition is shown in the following Figure:

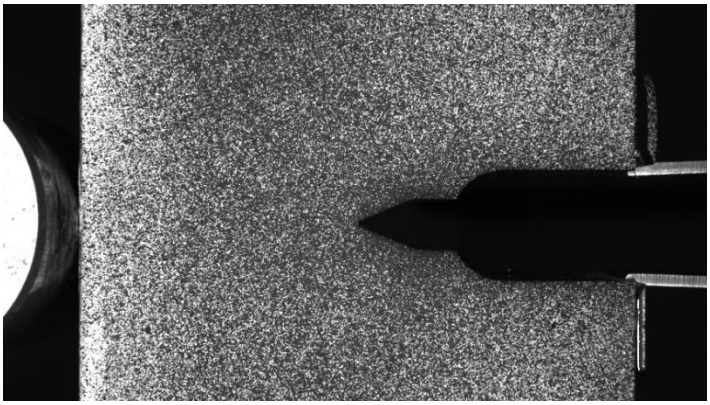

Figure 27. Initial condition of the test, image 0001

5.1. Comparison between DIC and extensometer

In order to verify the DIC method, this is first used to calculate the COD at some relevant times in the test, and the result is compared with the same value as obtained from the extensometer opening. Seeing the coordinates of the point of maximum force before an Unload in Figure 28 (Displacement=1.155857 [mm], Force= 43724.5 [N]) and comparing it with the values given in the test is possible to see that it corresponds to the time 113 [s] (the corresponding image would be image number 113, corresponding to Unload 15).

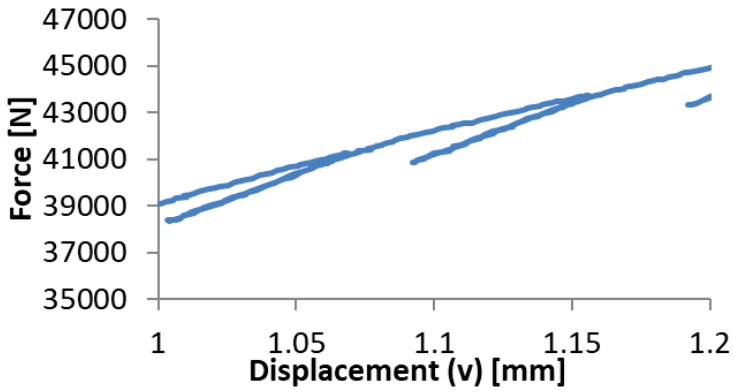

Figure 28. Zoom of Unload 15

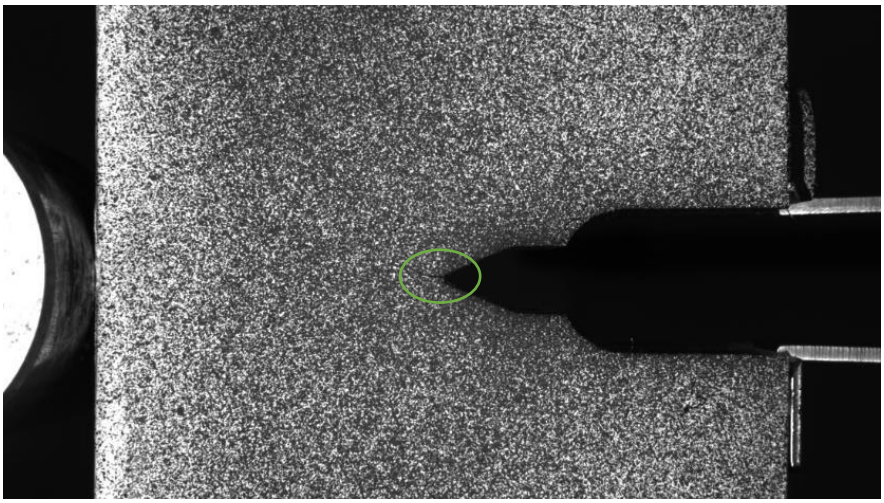

Figure 29. Crack growth on Image 0113

Using the undeformed image (Figure 27) and the image taken at time 113 [s] (Figure 29) the analysis of deformations on DICe is carried out. The configurations to make the calculation such as analysis mode, step size and subset size are indicated in Table 10.

Analysis mode	Subset-based full-field
Subset size	51 pixels
Step size	15 pixels

Table 10. Simulation Options

Two points of interest are added as close as possible to the strain gauge in order to obtain the results of the vertical displacements of these two points (see Figure 30). The algebraic difference of the y displacements of the points will be made in order to compare them to the COD values given in Table 4, in order to prove the accurateness of the DIC method.

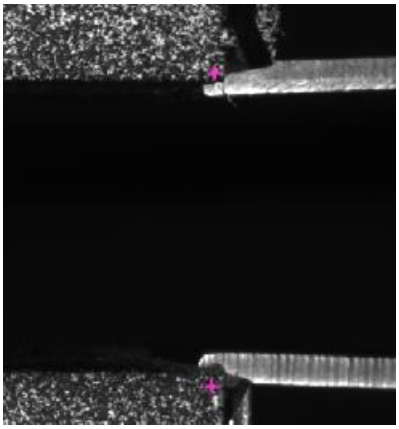

Figure 30. Placement of Point 0 (Upper) and Point 1 (lower) on the image

The results of DIC calculation are given in terms of pixels (point 0: -8.139, point 1: 10.626). To transform this result in [mm] it is considered the width 'W' given in Table 4. Considering the step size, it is obtained that each pixel corresponds to 0.0264 [mm].

In addition, the previous procedure is repeated for the first 20 Unload steps and the results are reported in Table 11.

Unload number	Extensometer	COD DIC	% Variation
1	0.085	0.050	-41.18%
2	0.113	0.082	-27.4%
3	0.141	0.102	-27.7%
4	0.169	0.131	-22.5%
5	0.197	0.163	-17.3%
6	0.226	0.176	-22.1%
7	0.256	0.218	-14.8%
8	0.286	0.241	-15.7%
9	0.318	0.277	-12.9%
10	0.350	0.308	-12%
11	0.383	0.333	-13.1%
12	0.419	0.375	-10.5%
13	0.459	0.407	-11.3%
14	0.502	0.449	-10.6%
15	0.553	0.495	-10.5%
16	0.614	0.546	-11.1%
17	0.682	0.617	-9.5%
18	0.752	0.673	-10.5%
19	0.826	0.746	-9.7%
20	0.907	0.803	-11.5%

Table 12. COD obtained from Sperimental Test vs calculated in DICe for the first 20 Unload steps

5.2 J Integral calculation

The J-integral calculation is made immediately before unloading steps, so as to allow comparison with the Standard method (see the red dots in Figure 31 as a reference). The calculation performed on image 113 is discussed here as an example.

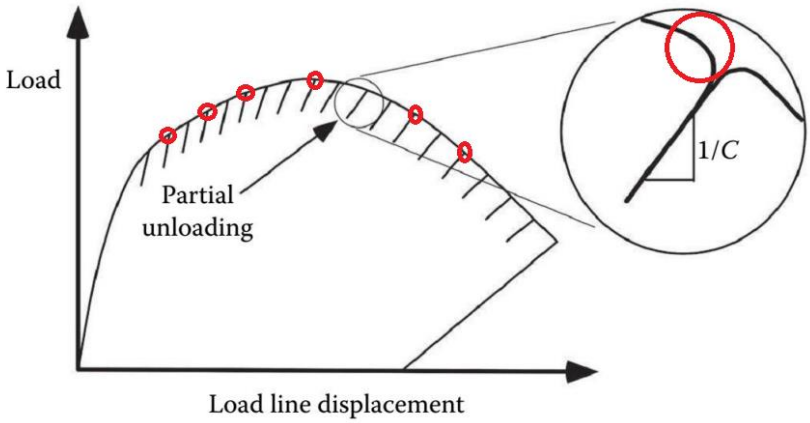

Figure 31. J-integral points of calculation on R-curve

As shown in Figure 32 the region of interest is chosen to enclose the most of the surface to have the highest freedom as possible for the election of the integration path. The boundaries are:

X0 = 220 pixels Xf = 1730 pixels
Y0 = 30 pixels Yf = 1040 pixels

An exclusion zone is added in the crack so to avoid unnecessary calculation.

It was found that the DIC options used in Table 10 were not accurate enough to obtain the desired J value, so a smaller step size and subset size were chosen in order to obtain better accuracy as shown in Table 13.

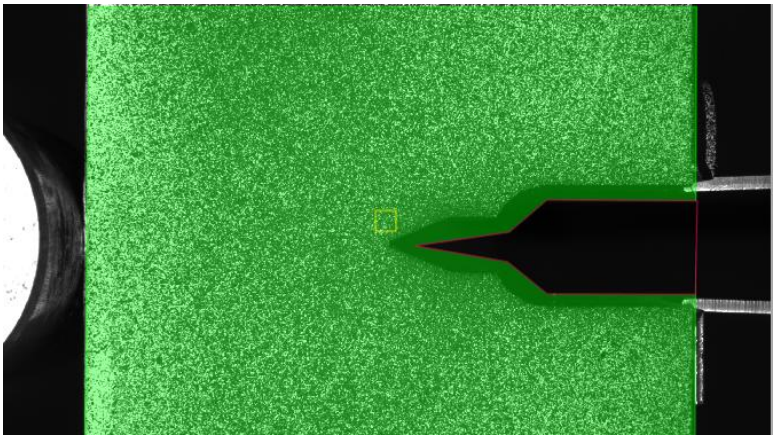

Figure 32. Region of Interest chosen for tracking

Analysis mode	Subset-based full-field
Subset size	31 pixels
Step size	10 pixels

Table 13. Simulation Options

The txt file produced by DICe consists of a Table (see Table 14) containing the coordinates in x and y direction of each subset with a separation depending of the step size. Other data produced in the txt file such as sigma, gamma, status flag and uncertainty are not indicated here as they are a representation of the accuracy of the calculation and are not important for this analysis.

Subset _ID	COORDINATE_ X	COORDINATE_ Y	DISPLCEMENT_ X	DISPLACEMENT_ Y	VSG_STRAIN_ XX	VSG_STRAIN_ YY	VSG_STRAIN_ XY
0	2.2000E+002	1.0400E+003	-8.2163E+000	-6.6870E-001	9.3865E-004	-3.5545E-003	-5.9954E-004
1	2.2000E+002	1.0300E+003	-8.1425E+000	-6.2974E-001	8.9107E-004	-3.4622E-003	-1.0911E-003
2	2.2000E+002	1.0200E+003	-8.0602E+000	-5.8830E-001	7.0554E-004	-3.3076E-003	-1.8389E-003
3	2.2000E+002	1.0100E+003	-7.9754E+000	-5.5009E-001	5.5753E-004	-2.3879E-003	-2.1591E-003
4	2.2000E+002	1.0000E+003	-7.9008E+000	-5.3255E-001	6.6559E-004	-2.8527E-003	-1.9679E-003

Table 14. txt file produced by DICe

With the use of Matlab, the matrices of displacements and strains are created with the number of x elements in the columns and the number of y elements in the rows.

```
ux=zeros(102,152);
uy=zeros(102,152);
eps_xx=zeros(102,152);
eps_yy=zeros(102,152);
eps_xy=zeros(102,152);
```

With the number of subsets in the x direction and the width dimension indicated in Table 1 it is found that the scale of the system corresponds to 0.0264 [mm/pixel]. In Figure 33(a) is shown the image created of the object with each point representing a subset, while Figure 33(b) indicates the position of each subset in millimeters.

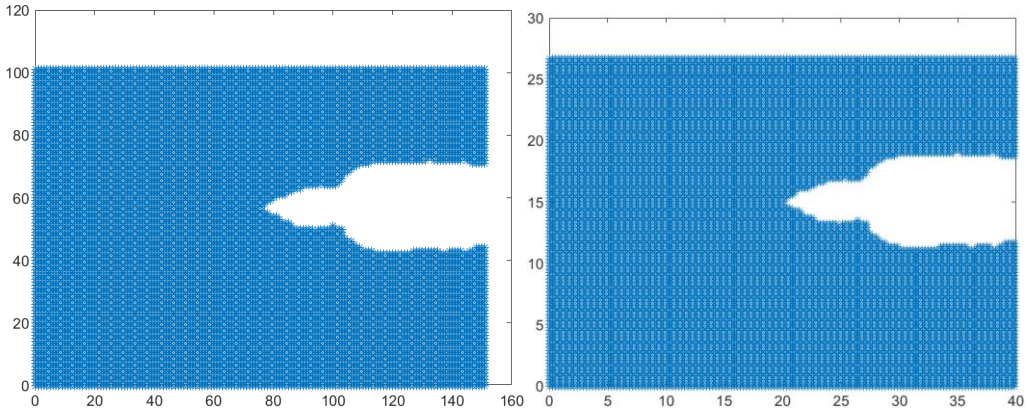

(a) *(b)*

Figure 33. Image of each subset position (a) and their position in [mm] (b)

The coordinate system that is implemented by DICe uses a vertical axis going downwards (which inverts the images from Figure 33 but does not influence on the final result).

Once finished the first column it continues with the second one starting from the same y coordinate going downwards and so on.

Based on this, the following loop is created to order the displacements x and y, and strains in xx, yy and xy directions:

```
for i=1:length(COORDINATE_X)
      ux(1+(COORDINATE_Y(i)-30)/10,1+(COORDINATE_X(i)-220)/10)=DISPLACEMENT_X(i)*scale;
      %[mm]
      uy(1+(COORDINATE_Y(i)-30)/10,1+(COORDINATE_X(i)-220)/10)=DISPLACEMENT_Y(i)*scale;
      %[mm]
      eps_xx(1+(COORDINATE_Y(i)-30)/10,1+(COORDINATE_X(i)-220)/10)=VSG_STRAIN_XX(i);
      eps_yy(1+(COORDINATE_Y(i)-30)/10,1+(COORDINATE_X(i)-220)/10)=VSG_STRAIN_YY(i);
      eps_xy(1+(COORDINATE_Y(i)-30)/10,1+(COORDINATE_X(i)-220)/10)=VSG_STRAIN_XY(i);
end
```

In Figure 34 are indicated the plots of the previous DIC variables. As the test is carried out the object is subjected to a deflection that tends to open the crack, so the extremities tend to open and move towards the left, as can be seen in the displacements from the plots from Figure 34 (A) and (B).

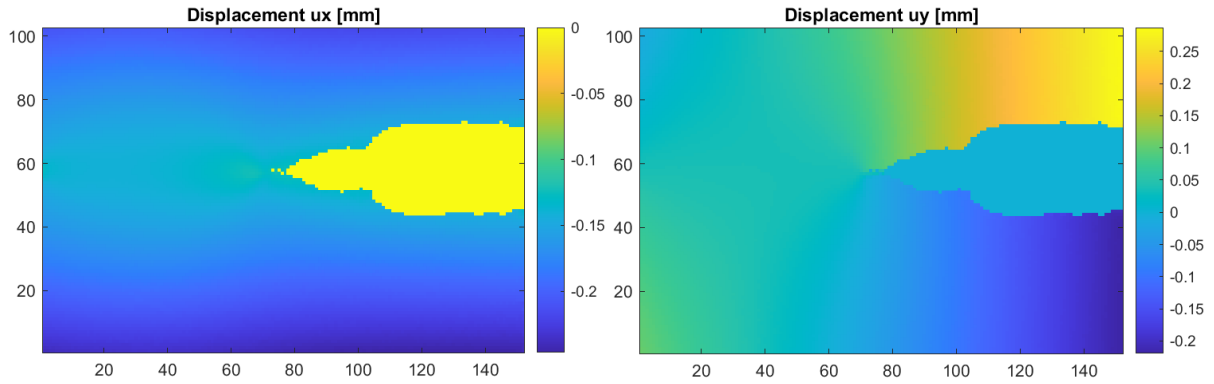

(A) Horizontal Displacement *(B) Vertical Displacement*

Figure 34. Plots of x (A), y (B) Displacements for calculation of Image 113 vs Image 001

Directly ahead of the crack tip (along the crack plane), the strain ε_{xx} is typically positive, indicating tensile strain due to the opening of the crack (see Figure 35 (A) and (B)), while directly behind the crack tip, ε_{xx} can be negative due to compressive effects as the crack faces pull apart and induce a compressive strain in the material behind the crack tip. Above and below the crack tip (perpendicular to the crack plane), the strain ε_{xx} is generally positive, indicating the material is being pulled apart in the vertical direction. The same assumptions can be made when analyzing the strain ε_{yy} (Figure 35 (C) and (D)).

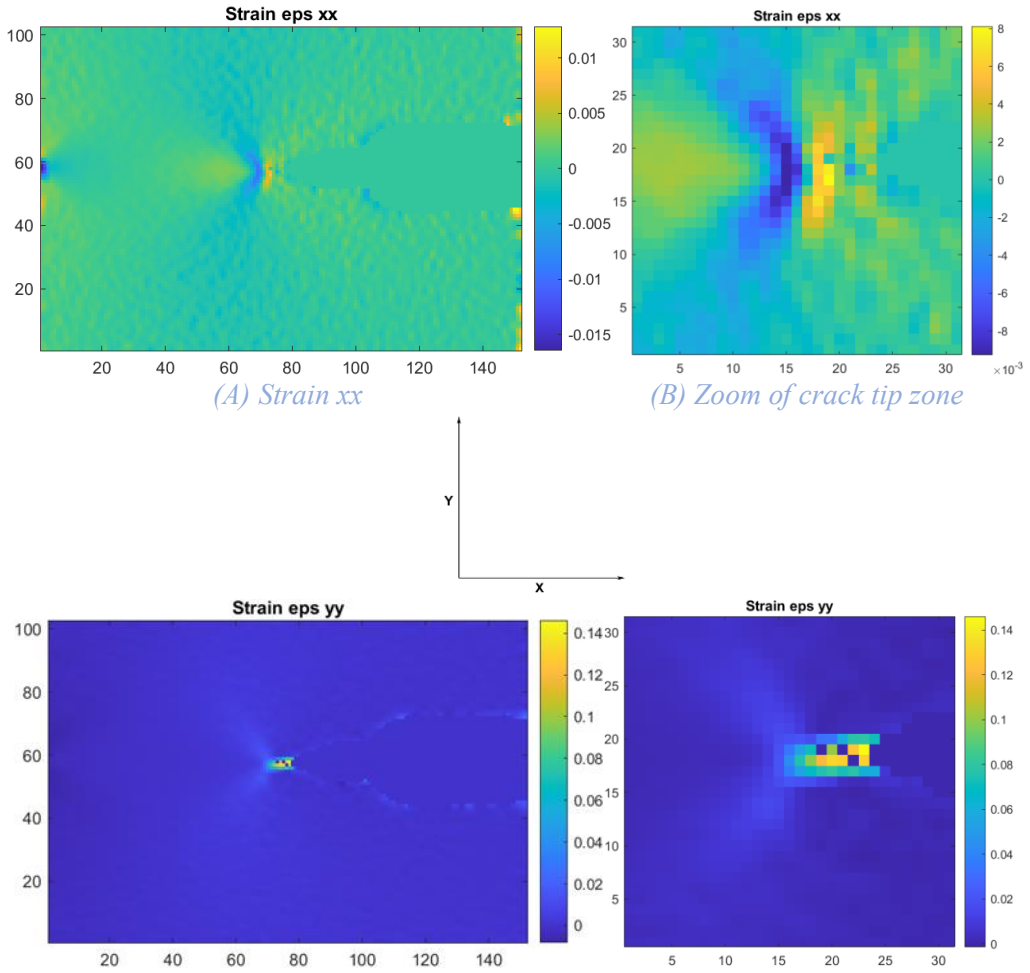

(A) Strain xx *(B) Zoom of crack tip zone*

C) Strain yy *(D) Zoom of crack tip zone*

Figure 35. Plots of Strain xx (A) and yy (C), and focus of Strain xx (B) and yy (D) over the crack tip for calculation of Image 113 vs Image 001

Directly ahead of the crack tip, the ε_{xy} strain is generally zero. This is because there is no shear strain in the plane directly ahead of the crack tip. Further ahead the crack tip, the ε_{xy} strain is also generally zero due to the symmetry of the loading condition. Above and below the crack tip, the ε_{xy} strain tends to be non-zero, indicating the presence of shear strain. The sign and magnitude of this shear strain depend on the exact angular position around the crack tip (See Figure 36).

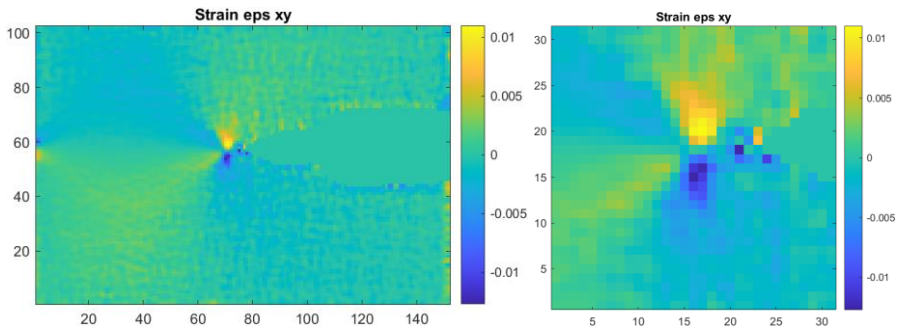

(A) Strain xy *(B) Zoom of crack tip zone*

Figure 36. Plots of Strain xy (A), and focus of Strain xy over the crack tip for calculation of Image 113 vs Image 001

After analyzing the previous variables, the stresses can be calculated using an elastic-perfectly plastic material model [10].

Two assumptions are made in order to compare the results, first with plane strain and then with plane stress.

5.3 Calculation of the stresses and energy with the Plane srain assumption

Plane strain assumptions can provide very good representations of real life components. Essentially, the in-plane strains are developed as in the full 3D formulation, but the out-of-plane or z-direction strains are set to zero. This condition would exist in an object that is constrained in the z-direction by rigid walls; the formulation only allows the resolution of strain 'in (the) plane', hence the name 'plane strain' [11]:

$$\varepsilon_{zz} = \varepsilon_{xz} = \varepsilon_{yz} = 0$$

Plane strain assumptions tend to be a very good approximation of the behavior inside a thick component that is loaded only in one plane. The large amount of material through the thickness essentially renders through-thickness strain irrelevant (or at least negligible) [11].

Under plane strain conditions the Hooke's law takes the form

$$\begin{bmatrix}\sigma_{xx}\\ \sigma_{yy}\\ \sigma_{xy}\end{bmatrix} = \frac{E}{(1+\nu)(1-2\nu)}\begin{bmatrix}1-\nu & \nu & 0\\ \nu & 1-\nu & 0\\ 0 & 0 & 1-2\nu\end{bmatrix}\begin{bmatrix}\varepsilon_{xx}\\ \varepsilon_{yy}\\ \varepsilon_{xy}\end{bmatrix} \qquad \text{Eq. 28}$$

The potential energy density can be calculated as indicated in Eq. 6. In addition, the Von Mises stress assuming plane strain is calculated from Eq. 29 in order to evaluate whether each point of the material is Yielded or not.

$$\sigma_V = \sqrt{\sigma_{xx}^2 + \sigma_{yy}^2 - \sigma_{xx}\sigma_{yy} + 3\sigma_{xy}^2 - \nu(1-\nu)(\sigma_{xx}+\sigma_{yy})^2} \qquad \text{Eq. 29}$$

A study of local yielding is carried out. For each subset in the structure is calculated the local Von Mises stress and is compared with the Yield strength. If that value is higher than the yield strength correction factor has to be applied to the stresses in that point:

$$\sigma_{xx} = \sigma_{yy}\frac{\sigma_{YS}}{\sigma_{VM}} \qquad \text{Eq. 30}$$

$$\sigma_{yy} = \sigma_{yy}\frac{\sigma_{YS}}{\sigma_{VM}} \qquad \text{Eq. 31}$$

$$\sigma_{xx} = \sigma_{xy}\frac{\sigma_{YS}}{\sigma_{VM}} \qquad \text{Eq. 32}$$

Indicating that the material undergoes plastic deformation at those points. So, the elastic energy 'w' must also be corrected as function of the Yield strength (see Figure 37 and Eq. 3).

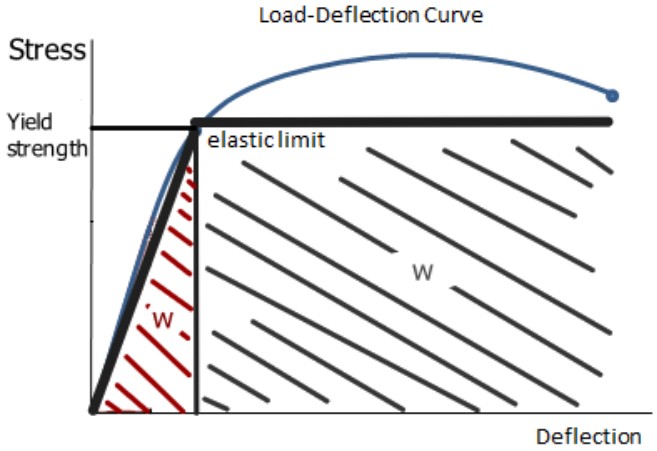

Figure 37. Elastic energy calculation for stresses higher than Yield strength

The red area indicates the elastic energy under elastic deformation. To that contribution it is added the strain energy under plastic deformation (black area):

$$w = \frac{1}{2}\frac{{\sigma_{YS}}^2}{E} + \sigma_{YS}\left(\frac{\sigma_{VM}-\sigma_{YS}}{E}\right) \qquad \text{Eq. 33}$$

The matlab code for the calculation of the previous variables is:

```
for i=1:102
    for j=1:152
        sig_xx(i,j)=E/((1+v)*(1-2*v))*((1-v)*eps_xx(i,j)+v*eps_yy(i,j)); %[N/mm2]
        sig_yy(i,j)=E/((1+v)*(1-2*v))*(v*eps_xx(i,j)+(1-v)*eps_yy(i,j)); %[N/mm2]
        sig_xy(i,j)=E/((1+v)*(1-2*v))*(1-2*v)*eps_xy(i,j); %[N/mm2]

w(i,j)=0.5*(sig_xx(i,j)*eps_xx(i,j)+sig_yy(i,j)*eps_yy(i,j)+2*sig_xy(i,j)*eps_xy(i
,j)); %[N/mm2]
        sig_vonMises(i,j)=sqrt(sig_xx(i,j)^2+sig_yy(i,j)^2-
sig_xx(i,j)*sig_yy(i,j)+3*sig_xy(i,j)^2);
        if sig_vonMises(i,j)>sig_ys
            sig_xx(i,j)=sig_xx(i,j)*sig_ys/sig_vonMises(i,j);
            sig_yy(i,j)=sig_yy(i,j)*sig_ys/sig_vonMises(i,j);
            sig_xy(i,j)=sig_xy(i,j)*sig_ys/sig_vonMises(i,j);
            w(i,j)=0.5*sig_ys^2/E+sig_ys*(sig_vonMises(i,j)-sig_ys)/E;
        end
    end
end
```

The results of the Von Mises stresses are compared to the Yield strength of the material indicated in Table 4. The superior limit on Figure 38 is set equal to this Yield strength (YS=

922 [MPa]), so all the values that surpass this limit are set equal to the Yield strength, as they represent nonrealistic values and just indicate whether the material is yielded at that point.

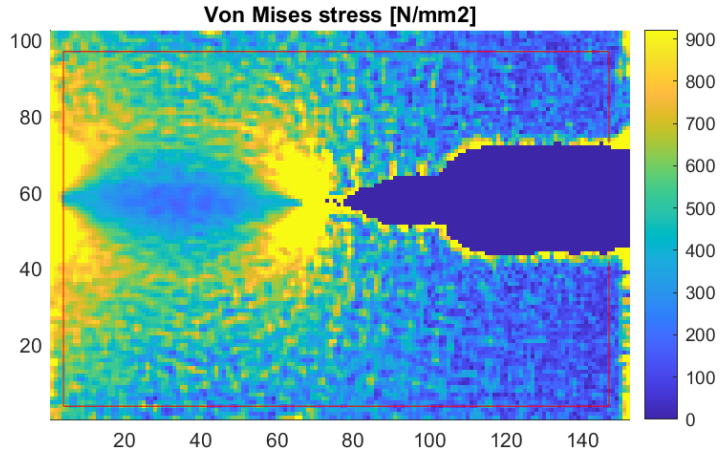

Figure 38. Von Mises stresses of calculation for Unload 15 and J-integral path

The same procedure to limit the stresses made previously is made for the stresses xx, yy and xy indicated in Figure 39.

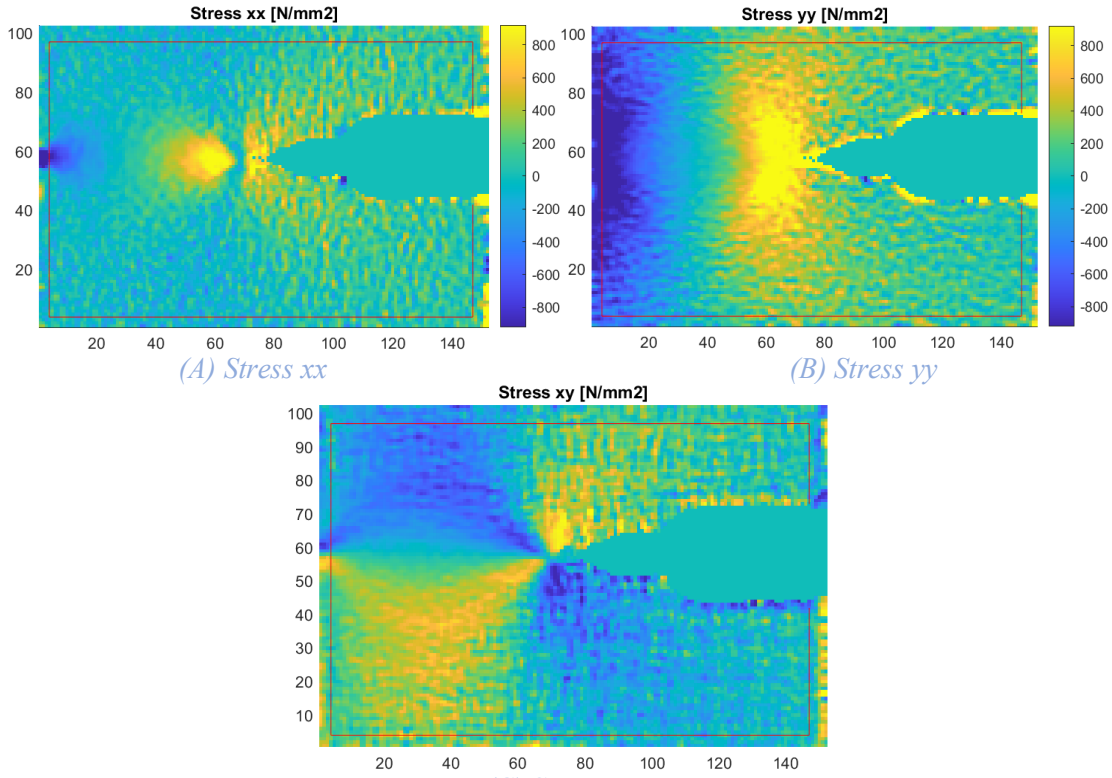

(A) Stress xx *(B) Stress yy*

(C) Stress xy

Figure 39. Plots of Stress xx (A), yy (B) and xy (C) for calculation of Image 113 vs Image 001

5.4 Integration

For a rectangular path as the one seen in Figure 40 (as the one chosen for this project) Eq. 5 can be simplified subdividing the integral into horizontal and vertical paths:

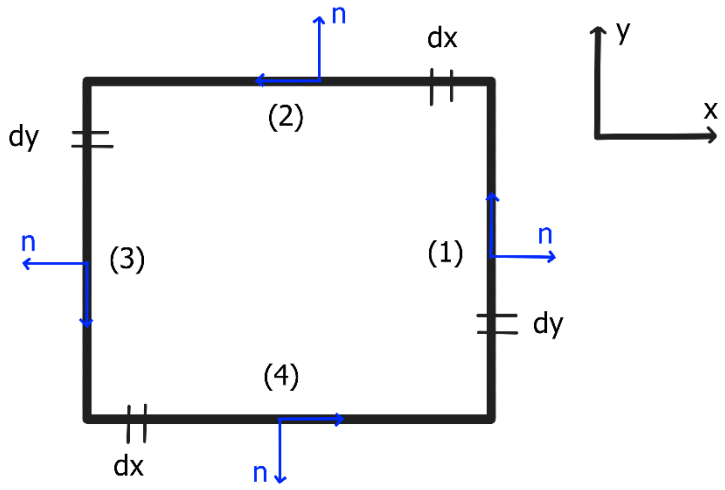

Figure 40. Subdivision of the different paths for integration over a rectangle

- Vertical path (path 1)

$$n = (1,0) \rightarrow n_y = 0,\ n_x = 1$$
$$ds = dy$$
$$T = [\sigma][n] = (\sigma_{xx}, \sigma_{xy})$$

J integral for the vertical path becomes:

$$J = \int_\Gamma \left[w dy - \left(\sigma_{xy}\varepsilon_{xx} + \sigma_{yy} * \frac{\partial uy}{\partial x} \right) dy \right] \qquad \text{Eq. 34}$$

This formula is referred for a vertical path pointing upwards. For the vertical path going downwards (path 3) the formula is the same but multiplied by -1.

- Horizontal path (path 2)

$$n = (0,1) \rightarrow n_x = 0$$
$$dy = 0$$
$$ds = dx$$
$$T = (\sigma_{xy}, \sigma_{yy})$$

J integral for the horizontal path becomes:

$$J = \int_\Gamma \left[- \left(\sigma_{xy}\varepsilon_{xx} + \sigma_{yy} * \frac{\partial uy}{\partial x} \right) dx \right] \qquad \text{Eq. 35}$$

This formula is referred for a horizontal path going to the left. For the horizontal path going to the right (path 4) the formula is the same but multiplied by -1.

The values of dux/dx in Eq. 12 correspond to the strain ε_{xx}, while the values of duy/dx are calculated with the denominator as δx and the numerator as the difference between two consecutive values of uy from the same row.

```
for i=1:102
    for j=1:151
        duy_dx(i,j)=(uy(i,j+1)-uy(i,j))/10;
    end
end
```

Considering the dimensional limits of the analysis the path to calculate the J integral is set as indicated in Figure 41. Each 'X' represents the corners of the rectangle with the respective coordinates.

J1 -> J for the path (1)
J2 -> J for the path (2)
J3 -> J for the path (3)
J4 -> J for the path (4)
J5 -> J for the path (5)

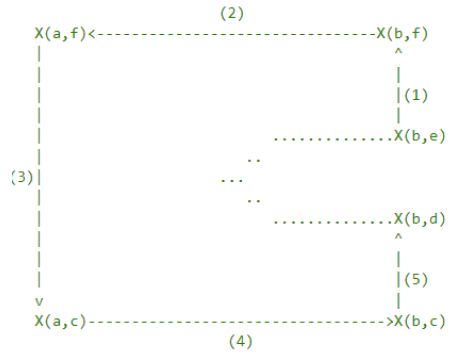

Figure 41. Integration path coordinates

The values of 'e' and 'd' are constant, as they represent the position of the intersection of the path with the crack edges (d=43, e=71). The following considerations to choose the integration path are taken into account:

1. The integration path has to be as far as possible from the large strain zone. i.e. From the crack tip.

2. Leave a couple of pixels between the border of the piece and the integration path, in order to avoid calculation errors due to boundaries. 4 pixels of space is chosen as a first try (see Figure 42). The first calculation for Unload 15 is carried out with this consideration and the results obtained are:

Unload number	J integration [kJ/m2]
Unload 15	127.62

Table 15. J integration value first try for Unload 15

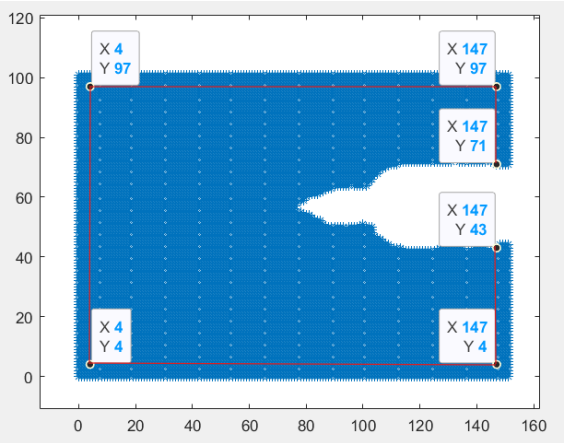

Figure 42. Integration path first try Unload 15

3. It was observed that moving the path (3) to the right slightly increases the J value. Some examples of how J changes by modifying the 'a' value (horizontal position of path (3)) are given in the following Table:

"a" value	J integral [kJ/m2]
a=4	127.62
a=5	125.88
a=6	129.41
a=10	132.51
a=15	134.99
a=25	134.38

Table 16. J integral values changing the path (3) position for Unload 15

By changing the other path values (b, c and f) the changes in the J integral are again negligible (see Tables 17, 18 and 19), which confirms the theory of the path independence of the J integral.

"b" value	J integral [kJ/m2]
b=135	119.99
b=140	123.63
b=145	125.37
b=146	123.25
b=147	127.62
b=148	133.21

Table 17. J integral values changing the path (1) position for Unload 15

"c" value	J integral [kJ/m2]
c=3	138.07
c=4	127.62
c=5	122.68
c=6	129.26
c=10	130.99
c=15	132.59
c=20	129.18

Table 18. J integral values changing the path (4) position for Unload 15

"f" value	J integral [kJ/m2]
f=100	126.88
f=99	120.66
f=98	123.30
f=97	127.62
f=96	125.61
f=90	121.23
f=85	125.24
f=80	125.67

Table 19. J integral values changing the path (2) position for Unload 15

It is thus demonstrated that the calculated J values is nearly path-independent as expected.

In addition, the same procedure carried out for Unload 15 is repeated from Unload 10 to 25, as seen in Table 20.

	J standard test method [KJ/m2]	J integration [KJ/m2]
Unload 10	41.4	54.09
Unload 11	48.8	61.19
Unload 12	58.4	80.87
Unload 13	68.3	88.84
Unload 14	81.6	105.43
Unload 15	97.1	127.62
Unload 16	114.5	143.96
Unload 17	136.8	187.95
Unload 18	160.9	214.54
Unload 19	183.8	237.13
Unload 20	209.8	246.68
Unload 21	241.0	291.51
Unload 22	267.3	349.98
Unload 23	296.4	356.86
Unload 24	320.0	365.01
Unload 25	352.2	402.14

Table 20. J integral obtained using the standard test method vs integrating for Unloads 10 to 25 for plane strain

5.5 Plane stress

Plane stress, on the other hand, assumes that the three stress tensor components relating to the z-direction are zero (see Eq.36). This is, of course, never actually the case inside of a real part, but the approximation trends towards applicability as thickness of the component approaches zero; there is not enough bounding material to maintain the through-thickness stress:

$$\sigma_{zz} = \sigma_{xz} = \sigma_{yz} = 0$$

This is great for analyzing very thin plates that are loaded only in the plane, but it can also be applied to the surface of thicker components. In fact, the surface of a plate is the only location where true plane stress conditions can exist. It is a perfect representation of the boundary condition [11].

$$\begin{bmatrix} \sigma_{11} \\ \sigma_{22} \\ \sigma_{12} \end{bmatrix} = \frac{E}{1-\nu^2} \begin{bmatrix} 1 & \nu & 0 \\ \nu & 1 & 0 \\ 0 & 0 & \frac{1-\nu}{2} \end{bmatrix} \begin{bmatrix} \varepsilon_{11} \\ \varepsilon_{22} \\ 2\varepsilon_{12} \end{bmatrix} \quad \text{Eq. 36}$$

The same path is chosen for this case, as shown in Figure 45 for the J integration. The same procedure is repeated for the calculation from Unloads 10 to 25 (see Table 21).

	J standard test method [KJ/m2]	J integration [KJ/m2]
Unload 10	41.4	46.05
Unload 11	48.8	52.24
Unload 12	58.4	69.54
Unload 13	68.3	76.52
Unload 14	81.6	92.22
Unload 15	97.1	110.98
Unload 16	114.5	127.07
Unload 17	136.8	168.29
Unload 18	160.9	192.86
Unload 19	183.8	212.92
Unload 20	209.8	223.85
Unload 21	241.0	265.20
Unload 22	267.3	317.58
Unload 23	296.4	324.97
Unload 24	320.0	333.37
Unload 25	352.2	368.63

Table 21. J integral obtained using the standard test method vs integrating for Unloads 10 to 25 for plane stress

In Figure 43 is indicated the colored map of the Von Mises stresses for Plane stress condition.

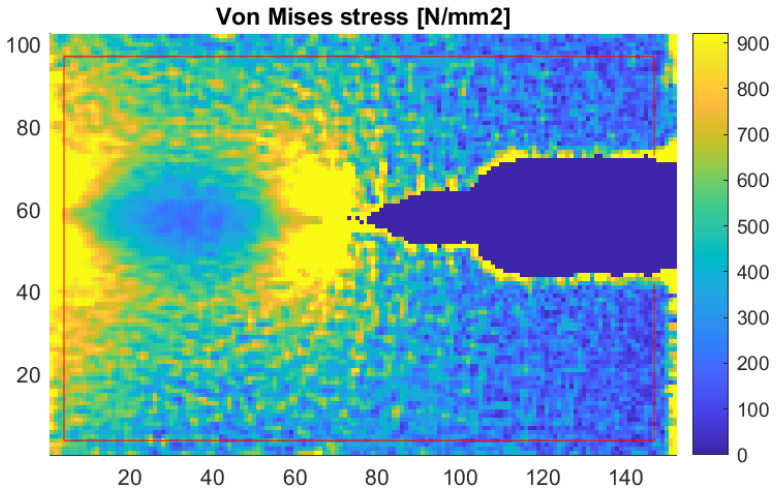

Figure 43. Von Mises stresses of calculation for Unload 15 and J-integral path Plane stress

5.6 Differences in J-Integral Calculation Plane Strain vs Plane stress

While it's typically expected that the strain energy density might be higher under plane strain for the same strain, in practice, calculations and specific material behaviors can show variations. Table 22 shows the comparison between the J integration values for the previous two cases considered and how consistently the integration values are higher in Plane strain.

	J integration Plane strain [KJ/m2]	J integration Plane stress [KJ/m2]
Unload 10	54.09	46.05
Unload 11	61.19	52.24
Unload 12	80.87	69.54
Unload 13	88.84	76.52
Unload 14	105.43	92.22
Unload 15	127.62	110.98
Unload 16	143.96	127.07
Unload 17	187.95	168.29
Unload 18	214.54	192.86
Unload 19	237.13	212.92
Unload 20	246.68	223.85
Unload 21	291.51	265.20
Unload 22	349.98	317.58
Unload 23	356.86	324.97
Unload 24	365.01	333.37
Unload 25	402.14	368.63

Table 22.Comparison between J integral obtained under Plane strain and Plane stress for Unloads 10 to 25

In plane stress, stress is assumed to be zero in the thickness direction (typically, the out-of-plane direction). This condition usually applies to thin structures like thin plates or shells, where the stress in the thickness direction is negligible due to the small dimension. The strain in the thickness direction is not constrained, so the material can expand or contract freely in that direction in response to loading.

The absence of significant constraint in the thickness direction means that the material's response to loading is somewhat "relaxed." As a result, the stresses in the in-plane directions (along the length and width of the structure) may be lower compared to a situation where the material is constrained.

In plane strain, strain in the thickness direction is assumed to be zero, which corresponds to a fully constrained situation in that direction. This typically applies to thick structures or cases where the material cannot deform in the out-of-plane direction, such as in long cylinders or deep beams. This constraint means that the material cannot expand or contract in the thickness direction, which introduces additional stress in the in-plane directions.

So the constraint on deformation increases the stiffness of the material, causing higher in-plane stresses. In other words, since the material is "locked" from deforming out-of-plane, it is forced to accommodate the load entirely through in-plane stress, leading to higher stresses compared to plane stress conditions and finally, higher J integral estimates.

5.7 Δa calculation

To complete the analysis, it has to be calculated the variation of crack length (Δa) in both Plane strain and Plane stress conditions, taking into account a visual analysis in DICe . The procedure is descibred in the following steps.

The u_y displacement chart from Figure 34 (B) evidences clearly the presence of the crack. Two halves are present, the upper one with positive displacement and the lower one with negative displacement, evidencing that the piece is separating in the crack.

The points in which the color difference is barely visible are then seen as points in which the material is not being separated yet. So the objective is to find the boundary where the colors stop being uniform and start being two completely different.

Figure 44 indicates some examples of different Unload steps where the crack tip is located.

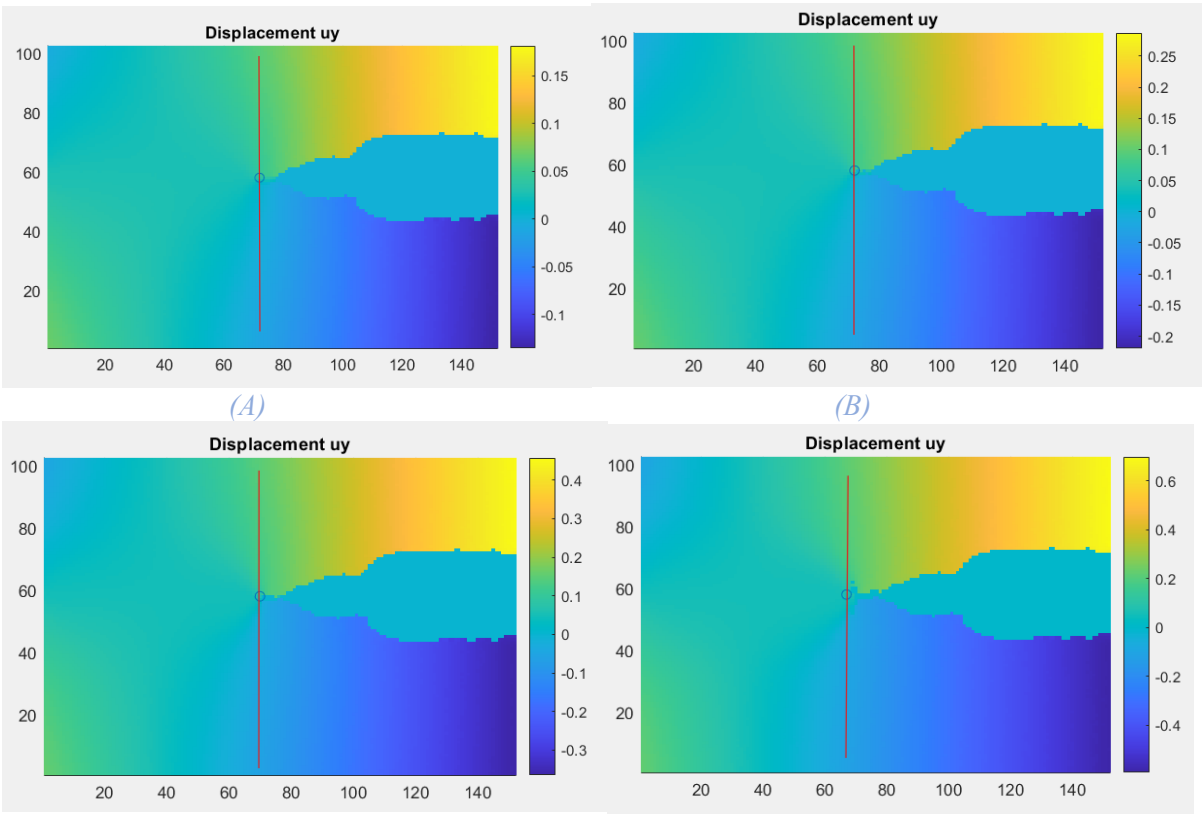

(A) *(B)*

(C) *(D)*

Figure 44. Crack tip localization on Unload 10 (A), 15 (B), 20 (C) and 25 (D)

Once found the points, it is located their horizontal position in terms of the subset number, to then being multiplied by the scale (x0.264 [mm/subset]).

The curve J-a obtained from the previous calculations is plotted in Figure 45.

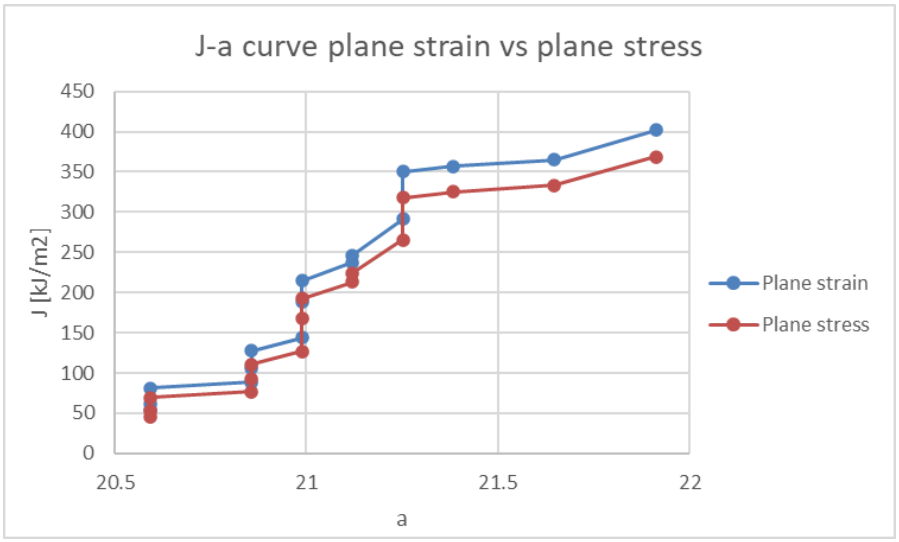

Figure 45. J-Δa curve comparing the results for Plane strain and Plane stress

The calculations from section 3.2 of the Standard Test method are repeated for the crack length previously measured, in order to calculate a_{0q} (for both Plane strain and Plane stress) and to interpolate J. In this way it is obtained the J integral curve for Plane strain and Plane stress with the interpolated 'a' values (see Figure 46).

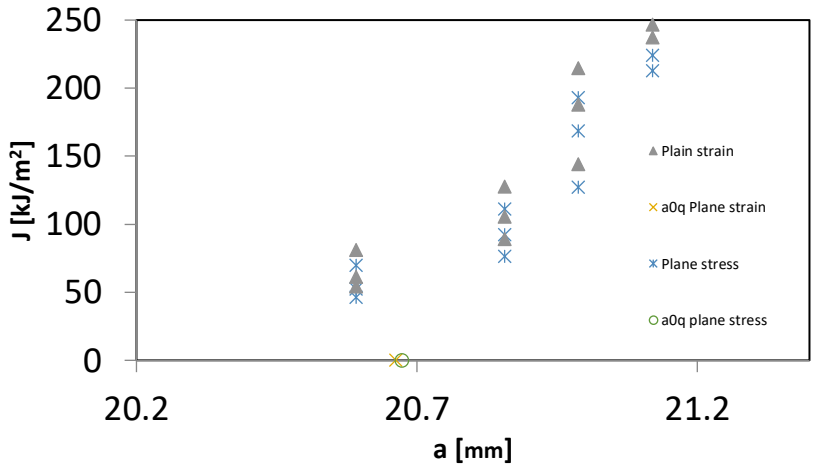

Figure 46. J-a curve comparing the results from DIC calculations using the J values in Plane strain and Plane stress.

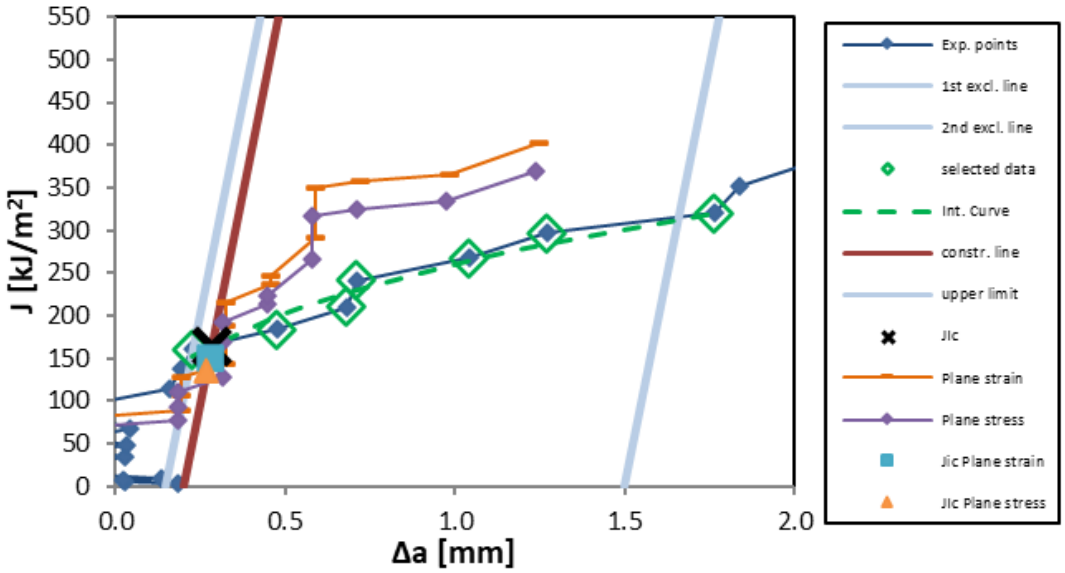

Figure 47. J-Δa curve comparing the results from DIC calculations, the Standard Test Method and the J values in Plane strain and Plane stress calculating crack length in DICe

It is possible to see the difference of the a_{0q} value for the three cases considered. An offset of around 1 [mm] is seen between the calculations using the crack length obtained by Fontana [1] and the approximations from DICe in Plane strain and Plane stress conditions.

In the case of J as seen in Figure 47, slight underestimation of the J-Δa curves is now seen compared to the Standard Test Method curve for low Δa values, while for higher ones there is an overestimation of J.

Table 23 compares the J_{Ic} values obtained from the previous analysis.

	Standard Test Method Test 44	DIC metho (Plane strain)	DIC metho (Plane stress)
J_{Ic}	164.6	150.62	134.68

Table 23. Comparison of the results of J_{Ic} for Standard Test Method of Test 44, Plane strain and Plane stress conditions

6. Conclusions

Elastic-plastic fracture mechanics provides a more comprehensive approach for analyzing fracture behavior in materials that exhibit significant plastic deformation. While linear elastic fracture mechanics is useful for materials where plasticity is limited to a small region near the crack tip, elastic-plastic fracture mechanics becomes essential when plastic deformation is more pronounced. The Crack Tip Opening Displacement and the J-integral are the two primary parameters used to assess fracture toughness in such cases.

J-integral offers an energy-based description of crack growth and is applicable to both linear and non-linear elastic materials. Its energy-based formulation provides valuable insights into the fracture process, making it a key tool in understanding the failure of elastoplastic materials.

It reflects different aspects of the fracture process, and their relationship depends on factors such as strain hardening and material constraints. As such, this parameter is crucial for designing and testing materials in structural applications where plastic deformation and fracture toughness are critical.

The research presented in this thesis focused on the analysis of the J-integral in fracture mechanics using Digital Image Correlation (DIC) techniques, by using the integral definition of J. The primary objective was to develop and validate a method for accurately measuring the J-integral through DIC, offering a non-contact, full-field approach that improves upon traditional techniques.

One of the main objectives is to present a reliable measurement technique of the J integral without the need of the Load/Unload procedure required in the Standard Test Method, as the data used (Figure 28) only take into account the peak Force at the beginning of each Unload step, which approximates a normal strain/stress curve.

This work underscores the importance of accurate crack length measurement and post-test verification in ensuring the validity of J_{IC} results, making it a valuable reference for materials testing and quality assurance in structural applications.

As far as the comparison between the different results obtained is concerned, the results of the Digital Image Correlation (DIC) analysis highlight a consistent underestimation of the Crack advancement when compared to the values obtained from the experimental Test. While for the J integral as seen in Tables 20 and 21 an overestimation for both cases is seen.

Once done the corresponding interpolation of the ‘a’ value, a slight underestimation of the J-Δa curves is now seen compared to the Standard Test Method curve for low Δa values, while for higher ones there is an overestimation of J.

In terms of the J_{IC} value, despite being in both Plane strain and Plane stress lower, the results are still close to the Standard Test method.

Several factors contribute to the observed discrepancies, such as Subpixel Interpolation and Resolution, Speckle Quality and Surface Preparation, Calibration and Optical Distortion or Strain Averaging.

Despite these challenges, the DIC method remains a valuable tool for displacement and strain measurement, especially given its versatility and non-contact nature. The slight variations in results can be mitigated by optimizing the experimental setup and improving factors like image resolution, calibration, and speckle pattern quality.

7. References

[1] Fontana, P. (2022). “Caratterizzazione meccanica di materiali metallici mediante tecniche di correlazione d’immagine”. [Master Thesis]. Politecnico di Torino.

[2] Anderson, T. (1988). “A Comparison of J-lntegral and CTOD as Fracture Toughness Parameters” in *Fracture Mechanics: Eighteenth Symposium*. ASTM SELECTED TECHNICAL PAPERS. pp 741-753.

[3] J.M. Vasco-Olmo, F.A. Díaz, F.V. Antunes, M.N. James, “Characterization of fatigue crack growth using digital image correlation measurements of plastic CTOD”, Theoretical and Applied Fracture Mechanics, Volume 101, 2019, Pages 332-341

[4] Rice, J.R., "A Path Independent Integral and the Approximate Analysis of Strain Concentration by Notches and Cracks." Journal of Applied Mechanics, Vol. 35, pp. 379-386, 1968.

[5] Griffith, A.A., "The Phenomena of Rupture and Flow in Solids," Philosophical Transactions, Series A, Vol. 221, pp. 163-198, 1920.

[6] ASTM E1820. (2023). *Standard Test Method for Measurement of Fracture Toughness*. pp. 4.

[7] R. Roberti, G.M. La Vecchia, D. Firrao, “Tenacità alla frattura di un acciaio legato per bonifica rinvenuto a temperature comprese tra 550 e 650°C”, La metallurgia italiana, Volume 81, n.5, 1989.

[8] Mathieu, F. (26 June 2023). “Digital Image Correlation- The Basics”. EikoSim. Available at https://eikosim.com/en/technical-articles/digital-image-correlation-the-basics/

[9] Elizabeth M. C. Jones, et. al. (October, 2018). “A Good Practices Guide for Digital Image Correlation: Standardization, Good Practices, and Uncertainty Quantication Committee”. INTERNATIONAL DIGITAL IMAGE CORRELATION SOCIETY. Pp. 5-28.

[10] Hooke’s law. (2024). Wikipedia. Available at https://en.wikipedia.org/wiki/Hooke%27s_law

[11] Fidelis. (n.d.). *Plane Stress vs Plane Strain – What Are They And Which Should You Choose?*. Available at https://www.fidelisfea.com/post/plane-stress-vs-plane-strain-what-are-they-and-which-should-you-choose